Journal of Nuclear Materials 518 (2019) 440–460

Contents lists available at ScienceDirect

Journal of Nuclear Materials

journal homepage: www.elsevier.com/locate/jnucmat

Hydrogen in zirconium alloys: A review

Arthur T. Motta [a, *], Laurent Capolungo [b], Long-Qing Chen [c], Mahmut Nedim Cinbiz [d], Mark R. Daymond [e], Donald A. Koss [c], Evrard Lacroix [a], Giovanni Pastore [f], Pierre-Clément A. Simon [a], Michael R. Tonks [g], Brian D. Wirth [h], Mohammed A. Zikry [i]

[a] Department of Mechanical and Nuclear Engineering, 138 Reber Bldg, Penn State University, University Park, PA, 16802, USA
[b] Materials Science and Technology Division, Los Alamos National Laboratory, Los Alamos, NM, 87545, USA
[c] Department of Materials Science and Engineering, The Pennsylvania State University, University Park, PA, 16802-5006, USA
[d] Reactor and Nuclear Systems Division, Nuclear Fuel Materials Group, Oak Ridge National Laboratory, Oak Ridge, TN, 37831, USA
[e] Dept. of Mechanical and Materials Engineering, Queen's University, Kingston, Ontario, K7L 3N6, Canada
[f] Idaho National Laboratory, Fuel Modeling and Simulation Department, Idaho Falls, ID, 83415, USA
[g] Department of Materials Science and Engineering, University of Florida, Gainesville, FL, 32611, USA
[h] Department of Nuclear Engineering, University of Tennessee, Knoxville, TN, 37996-1410, USA
[i] Dept. of Mechanical and Aerospace Engineering, North Carolina State University, Raleigh, NC, 27695-7910, USA

ARTICLE INFO

Article history:
Received 4 January 2019
Received in revised form
13 February 2019
Accepted 24 February 2019
Available online 2 March 2019

ABSTRACT

Hydrogen absorbed into zirconium alloy nuclear fuel cladding as a result of the waterside corrosion reaction can affect the properties of nuclear fuel, principally through the precipitation of brittle hydride particles. Multiple phenomena are involved in this overall process: after hydrogen pickup degradation of mechanical properties is controlled by hydrogen transport, hydride precipitation and dissolution kinetics and the formation of specific mesoscale hydride microstructures. The precipitation of hydrides especially affects cladding ductility and fracture toughness, but can also affect other phenomena, including via stress-induced hydride reorientation. These processes can affect cladding performance both during normal operation and during extended dry storage, as hydride morphology can be modified during the preparatory vacuum drying processes. We review the processes of hydrogen transport, hydride precipitation and dissolution and formation of mesoscale hydride microstructures, and highlight where more research is needed, both from an experimental and from a modeling point of view.

Contents

* Corresponding author.
E-mail address: atm2@psu.edu (A.T. Motta).

https://doi.org/10.1016/j.jnucmat.2019.02.042
0022-3115/

1. Introduction

In the reactor environment, the nuclear fuel cladding is exposed to a neutron flux which causes irradiation damage, in addition to thermal and mechanical-induced stresses which may drive component deformation, and to the coolant chemistry which causes corrosion and hydriding. The in-reactor residence times of nuclear fuel have increased from three to five years, as a direct consequence of the increase in fuel burnup from 30 to over 50 GWd/tHM [1]. This extended exposure entails end-of-life neutron fluences of greater than 10^{22} n.cm^{-2} (E > 1 MeV) which translates roughly to an increase in fuel cladding displacements per atom (dpa) from about 15 dpa to about 25 dpa. These atomic displacements result in changes to the microstructure of the material, including an increase in the dislocation loop density, and the dissolution of intermetallic particles [2–4]. These microstructural changes may degrade the cladding performance through mechanical property changes (hardening, embrittlement and loss of fracture toughness), dimensional changes associated with irradiation-induced deformation (creep and growth), and changes in corrosion resistance [5].

However, it is well known that the irradiation-induced hardening and embrittlement associated with radiation damage approximately saturate after about one month in the reactor [6]. Of potentially greater concern is the corrosion of the cladding tube by the reactor primary water and the associated hydrogen ingress into the zirconium cladding (commonly referred to as hydrogen pickup), which occurs during reactor operation. Both structural components and the nuclear fuel cladding used in the core of nuclear reactors are made of zirconium alloys. These alloys combine adequate mechanical properties with very low neutron absorption cross section [6].

Although Zr alloys generally exhibit very good high temperature corrosion resistance, they do undergo a slow uniform corrosion process by reacting with the coolant water on the outer surface of the fuel cladding material.

The zirconium alloy cladding reacts with water to form a protective layer of mostly monoclinic zirconium dioxide (the protective corrosion layer) according to the reaction:

$$Zr + 2H_2O \rightarrow ZrO_2 + 2H_2 \quad (1)$$

While this protective oxide layer does limit additional corrosion, it can reach thicknesses up to 100 μm at the end of life (representing a significant fraction of the wall thickness of ~600 μm for 17 × 17 assembly design). A variety of fuel rod and fuel assembly designs have been used throughout the years, including those containing duplex cladding, which although based on similar designs, are made of various alloys (e.g. Zircaloy-4, low Sn Zircaloy-4, Zircaloy-2, ZIRLO, M5, etc.) [7–9] and various cladding dimensions, and which have been subjected to a range of burnups and corrosion conditions.

This process results in the production of hydrogen, a small percentage of which enters the zirconium alloy component [10]. The result is a gradual increase in the total hydrogen concentration in the zirconium fuel cladding from the initial average hydrogen concentration value (as low as ~3 wt parts per million (wppm) for as-manufactured fuel cladding in recently manufactured fuel) to values as high as 600–700 wppm. An oxide thickness of 100 μm corresponds roughly to an overall hydrogen content of 800 wppm for a hydrogen pickup fraction of 15%.

Once the hydrogen solubility limit is exceeded, zirconium hydride platelets precipitate [12–14]. The presence of these hydride platelets can significantly affect cladding ductility even in the most favorable case when they precipitate homogeneously, and are aligned in the circumferential (in-plane) direction of the cladding tube [11,14,15]. The uniform elongation of these materials when tested at 250–300 °C can decrease to less than 1% due to early cracking of hydride particles or agglomerates. Furthermore, hydrogen is highly mobile in the fuel cladding and responds to concentration, stress and temperature gradients, leading to changes in hydrogen atom distribution and local maxima in hydride precipitate concentrations in the fuel rod. As a result of this hydrogen redistribution, hydrides may preferentially precipitate in a so-called "hydride rim" near the outer cladding surface [11,16] or in hydride blisters - if oxide spallation occurs creating a cold spot in the cladding [17,18]. Both these processes cause local increases in hydride concentration that can drastically reduce cladding ductility relative to a uniform hydride distribution [15,19]. The ductility is reduced even more if hydride precipitation happens under a sufficiently high hoop stress to cause hydride reorientation [20] as discussed below.

This review focuses on the formation of hydride particles during service, their modes of agglomeration and mesoscale structure formation and their effect on mechanical properties, as we believe this is a crucial issue for the use of zirconium cladded nuclear fuel. We note that this review is not exhaustive in discussing all the effects that hydrogen can have on zirconium cladding performance. Notably, the postulated effect of hydrogen on corrosion acceleration [16] and the observed effect of hydrogen in enhancing irradiation growth [21] are not discussed here. Also during high temperature transients such as during a postulated LOCA, the hydrogen content in the cladding affects the temperature and kinetics of the Zr-alloy crystallographic phase transformation from hcp alpha-phase to bcc beta-phase, lowering the onset of the transformation [22].

In the next section we review the processes of hydrogen pickup, transport within the cladding driven by concentration, temperature and stress gradients, followed by the mechanisms of hydride precipitation and dissolution and formation of mesoscale hydride morphology and the ultimate impact of the hydrides on cladding mechanical properties.

2. Hydrogen pickup

The hydrogen source of greatest concern is hydrogen pickup by the zirconium alloy cladding during the corrosion reaction, equation (1) [5,23,24]. In fact, although other sources of hydrogen exist, such as hydrogen water chemistry, only the hydrogen from corrosion is observed to enter the cladding [25]. The fraction of the total hydrogen generated during corrosion that gets picked up by the cladding is called the hydrogen pickup fraction f_H defined as

$$f_H = \frac{\Delta_0^t H_{absorbed}}{\Delta_0^t H_{generated}} \quad (2)$$

where $\Delta_0^t H_{absorbed}$ and $\Delta_0^t H_{generated}$ are the amount of hydrogen absorbed in the cladding and the amount of hydrogen generated from the start of corrosion exposure, respectively. Although often

taken as a constant, this quantity varies from alloy to alloy and varies during different stages of corrosion [23,26]. Fig. 1 shows the hydrogen content of different corrosion samples plotted versus weight gain (a measure of the degree of corrosion). The dotted lines in Fig. 1 show what those levels would be for different hydrogen pickup fractions f_H. If the hydrogen pickup fraction f_H were constant during corrosion, a linear function should be observed between weight gain and hydrogen pickup. In fact, it is clear from the plots that a linear relationship between weight gain (oxide formation) and hydrogen pickup is not followed, and that the hydrogen pickup fraction increases with increasing corrosion time for the alloys tested. It is also clear from the figure that the pickup fraction varies consistently between alloys [26].

The reasons for such differences in the pickup fraction between alloys have been extensively studied [10,27–31], focusing both on the transport mechanism of hydrogen through the protective oxide layer and on the driving force for this transport. It has been recently proposed that the driving force for hydrogen pickup is inversely proportional to the electronic conductivity of the protective oxide layer [32]. To close the reaction shown in equation (1), it is necessary for the electrons to travel through the protective oxide layer to recombine with the hydrogen in the water. If the oxide electronic conductivity is not sufficiently high, hydrogen can migrate through the protective oxide layer to recombine with electrons and be absorbed into the metal [32,33]. The transport mechanism of hydrogen through the oxide layer in response to this driving force is not yet determined, but it is now thought that hydrogen travels through the protective oxide as H^+ on the way to entering the metal [34–37].

The hydrogen that enters the metal can then migrate in response to concentration, temperature and stress gradients. This is the subject of the next section.

3. Hydrogen transport

The hydrogen that enters the cladding can respond relatively quickly to established driving forces which can drive a hydrogen flux to regions of the solid. The hydrogen flux due to the combined effects of Fick's law of diffusion, the Soret effect and stress is given by [38–42],

$$J_{diffusion} = J_{Fick} + J_{Soret} + J_{Stress} = -D_H \nabla C_{ss} - \frac{D_H C_{ss} Q^*}{RT^2}\nabla T + \frac{D_H C_{ss} V_H}{RT}\nabla \sigma_H \quad (3)$$

where C_{ss} is the hydrogen concentration in solid solution in the Zr matrix, Q^* is the heat of transport, D_H is the hydrogen diffusion coefficient [43], V_H the partial molar volume of hydrogen in Zircaloy, σ_H is the applied hydrostatic stress, R is the ideal gas constant and T is the temperature. To use equation (3), it is necessary to determine the diffusion coefficient D_H and the heat of transport Q^* [39] and to have information on the hydrostatic stress state.

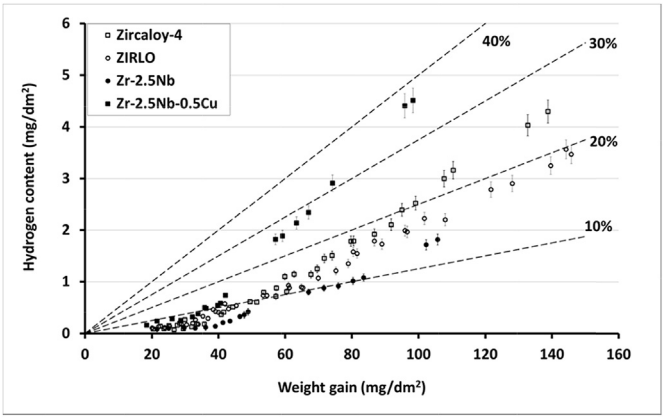

Fig. 1. Hydrogen content versus corrosion weight gain (proportional to oxide thickness) during autoclave testing of various alloys in pure water at 360 °C [23]. It is clear that a linear relationship is not followed and that the hydrogen pickup fraction varies consistently between alloys.

A stress gradient induces movement of hydrogen in a sample, as discussed by Ells and Simpson [44]. It has been shown that it is the hydrostatic stress component which drives movement of hydrogen [45], with a net flow towards tensile hydrostatic regions. This has most obvious practical importance when a flaw or notch-tip is present in the sample, in which case hydrogen is driven to the tensile stress concentration in front of the flaw [46,47]. If the flow of hydrogen 'up' the tensile stress gradient is sufficiently high then precipitation of hydrides (see Section 4.2) can occur at the stress-concentration location, even when the rest of the sample is below the terminal solubility limit.

The diffusion coefficient of hydrogen in zirconium, has been measured several times in the literature [48,49]. The experimental results first measured by Kearns [49] and calculated more recently by Zhang and co-workers [50] give the diffusion coefficient as:

$$D_H = 1.08x10^{-6}\exp\left(-\frac{0.46(eV)}{k_B T}\right) \quad \left[m^2/s\right] \quad (4)$$

where k_B is Boltzmann's constant and T is the temperature in Kelvin. Recent Monte Carlo simulations agree well with this result [51,52]. Incidentally, the calculations show that although hydrogen diffusion in Zircaloy is isotropic at room temperature, at higher temperature the rate of migration along the <c> direction in the hcp structure is higher than in the <a> direction [53].

The flux described by equation (3) results in a redistribution of hydrogen in the cladding. While the Fickian flux drives hydrogen from the outside of the cladding tube inwards, the Soret flux goes in the direction of decreasing temperature. In-reactor a steady heat flux is present from the inner to the outer radius so that hydrogen tends to migrate to the colder part of the fuel cladding, causing precipitation on the outside of the tube, often forming of a hydride rim (see Fig. 2 b) [54]. It is also possible to have azimuthal gradients caused for example by oxide spallation leading to a cold spot, in which case a hydride blister can form (see Fig. 2a) [55], see also Fig. 2 c. Finally in the axial direction, hydrogen has been shown to accumulate in the interpellet region where the heat flux is lower [40].

4. Hydride precipitation and dissolution

Once the hydrogen solubility in the alloy is reached, hydride platelets can precipitate within the alpha Zr matrix. These hydrides can be observed using metallographic techniques. These micrographs are normally obtained by chemical etching the sample to reveal the hydride particles. It is important to note that the hydrides observed after etching the sample when the sample is observed at low magnification are actually collections of smaller hydride particles aligned into a mesoscale structure as discussed below (see Fig. 28 and Fig. 29). It is the mesoscale hydride clusters that can influence and degrade mechanical properties, but many of the phenomena we describe, including the orientation relationship between hydride and matrix are applicable to the individual hydride particles.

The volume fraction of hydrides formed depends on the total concentration of hydrogen in the alloy and the alloy's Terminal Solid Solubility (TSS) for hydrogen. The concentration of hydrogen in solid solution in zirconium alloys at the TSS is small: less than 1 wt ppm at room temperature, reaching 65 wt ppm at ~310 °C, and

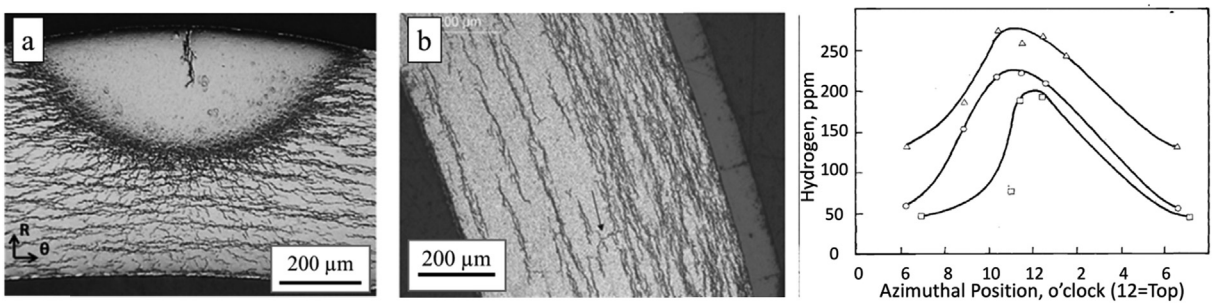

Fig. 2. Images of hydride microstructures which can be present in the zirconium alloys during the life cycle of a nuclear fuel rod (a) hydride blisters [56], (b) hydride rim [57], and (c) hydrogen content as a function of azimuthal position.

below 120 wt ppm at maximum operating temperatures, of about 340 °C [58–62]. Since hydrogen is highly mobile in zirconium alloys [50], it can respond reasonably quickly to temperature and stress gradients that drive it to precipitate preferentially in the regions of high hydrostatic tensile stress and low temperature.

Even without any imposed temperature or stress gradients, it has long been recognized that the texture of zirconium alloys has a strong impact on the orientation of precipitated hydrides [64]. The normally observed hydride is the face-centered cubic (fcc)-delta phase, although other phases are observed in different circumstances [65]. The precipitation process is affected by many factors, including the presence of grain boundaries, internal stresses and alloying elements. Moreover, hydride precipitation causes matrix strain, creating an elastic strain field around it that favors precipitation of other hydride particles nearby. This coupling leads to "macroscopic" hydride particles that are composed of a sum of much smaller microscopic hydrides arranged in a "deck of cards" configuration, as shown schematically in Fig. 10.

The solubility of hydrogen in zirconium alloys has been extensively studied. Early on, researchers identified that the solubility limit for hydride *dissolution* was different from that for hydride *precipitation* [66]. This is thought to be because the energy needed for hydride nucleation when cooling from high temperature requires undercooling to be present before precipitation can occur [67,68]. Many researchers have investigated hydride precipitation and dissolution as a function of temperature. Some of these results are summarized in Fig. 4, which shows various data collected for the terminal solid solubility during dissolution and for the terminal solid solubility during precipitation. This data has been principally obtained using differential scanning calorimetry and synchrotron radiation diffraction, as these two experimental methods are sensitive to the precipitation/dissolution reactions as they occur.

Differential scanning calorimetry (DSC): DSC is a non-destructive thermal analysis technique through which it is possible to follow a phase transformation within a sample by measuring the heat evolved by the exothermic precipitation transformation induced by the heat treatment, as revealed by the heat that needs to be supplied to a reference sample in which no precipitation occurs. Fig. 5 shows the output of such an experiment, in which a hydride sample containing 46 wppm hydrogen was heated from room temperature to 350 °C, at which temperature according to Fig. 4 all of the hydrogen is dissolved into the matrix. To maintain the heat flow constant between the sample of interest and a standard sample without hydrogen, heat must be provided to the sample that does not contain hydrogen to compensate for the heat of reaction in the hydrided sample. This heat flow is plotted in Fig. 5. As the temperature is increased more heat must be provided until the hydrogen is completely dissolved. The second curve shown is the

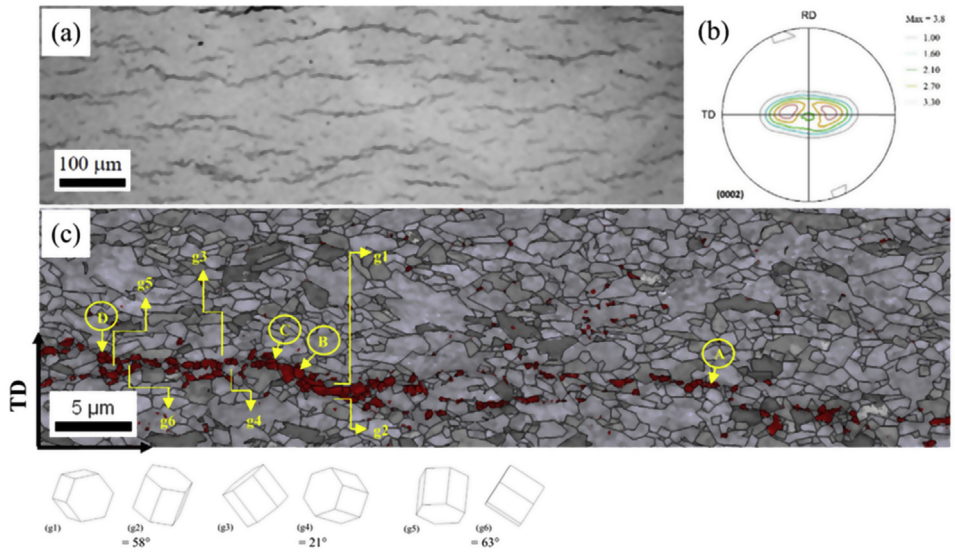

Fig. 3. (a) Optical micrograph of hydrogen-charged Zircaloy-4 (samples were etched to reveal hydrides), (b) crystallographic texture of Zircaloy-4 from basal plane pole figure, and (c) misorientation angles of grain boundaries between δ hydride and the α zirconium grain. (alpha Zirconium: gray tones and delta hydride: red) [63]. (For interpretation of the references to colour in this figure legend, the reader is referred to the Web version of this article.)

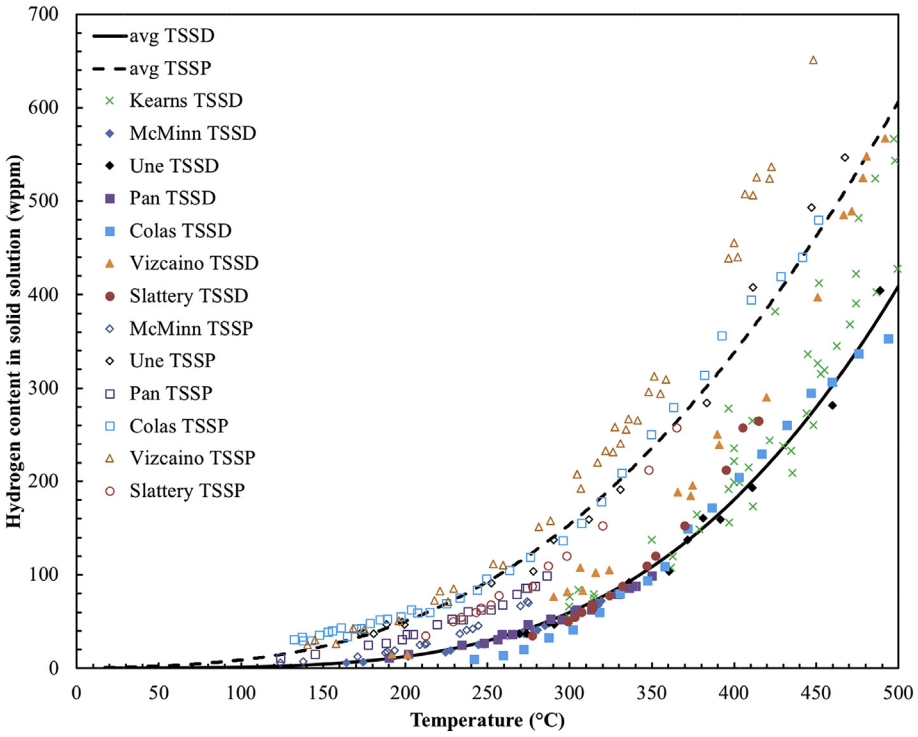

Fig. 4. Collection of data showing the terminal solid solubility for dissolution (TSSd) and for precipitation (TSSp) [13,58,61,62,69–71].

derivative of the first with respect to temperature; the maximum derivative point is usually taken as the point at which the reaction is completed, commonly referred to as the maximum slope temperature (in this case 284 °C).

Synchrotron radiation diffraction: High energy synchrotron x-ray radiation has been increasingly used to study hydride precipitation [59,67,70,72–75]. Synchrotron light sources can generate high-energy x-rays (such as 80 keV) with high brilliance (number of photons per second within a solid angle and within an energy band), which allows interrogation of the samples in transmission mode and to resolve small volume fraction phases such as hydrides in zirconium alloys as shown schematically in Fig. 6. Using such a geometry, diffraction rings from both the Zr matrix and the hydride phase can be detected. Because this experiment can be done using a furnace and the mechanical testing frame, the intensity of the hydride diffraction rings can be followed as a function of temperature

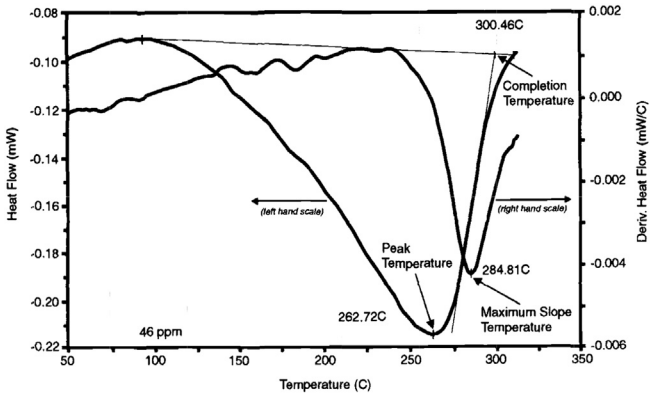

Fig. 5. Heat Flow versus temperature during testing of a Zircaloy-4 sample containing 46 wppm of Hydrogen during constant heating. After McMinn [58].

and applied stress. This is shown in Fig. 7 which illustrates the hydride diffraction signal from a sample containing 530 wppm hydrogen. As the temperature is increased (red line), the hydride diffraction intensity decreases, until reaching zero at complete dissolution, in this case 535 °C, in agreement with Fig. 4. After a brief hold at temperature, the temperature is again decreased and the hydride phase reprecipitates at the precipitation temperature given by TSSp, in this case about 450 °C. In such a manner the curves in Fig. 4 can be obtained [70]. The study of the hydride d-spacing and the full-width at half maximum of the diffraction peaks can give further information on the precipitation mechanisms [76].

4.1. Hydride morphology under zero stress

The morphology and spatial distribution of hydrides are crucial for understanding fracture initiation, and thus for improving the long-term stability of Zr-alloys in service. As mentioned above the phase diagram shows the stable hydride phase at low temperature as the fcc delta hydride phase, which is the phase normally observed experimentally [77–79], although other phases, notably the gamma phase, are occasionally observed, especially at the start of precipitation [65]. The basic properties of the delta and gamma phases are shown in Table 1. Other phases, including the eta -hydride [77] and the zeta −phase [80] have also been reported.

The delta hydrides form within the alpha zirconium matrix with the orientation relationship of (0001)hcpZr//(111) delta [77]. The different crystal structure and lattice constant of the delta hydride phase with respect to the alpha Zr matrix induces strain in the material. The stress caused by this strain induces the hydrides to form a disc shape that lies parallel to the basal plane of the α Zr hcp structure. The hydride surface energy may also be anisotropic, contributing to this platelet shape, but this is not certain as the surface energy is yet to be determined. The elastic stress field surrounding these nanoscale hydride discs favors precipitation of other hydride particles nearby. This coupling leads to “mesoscale”

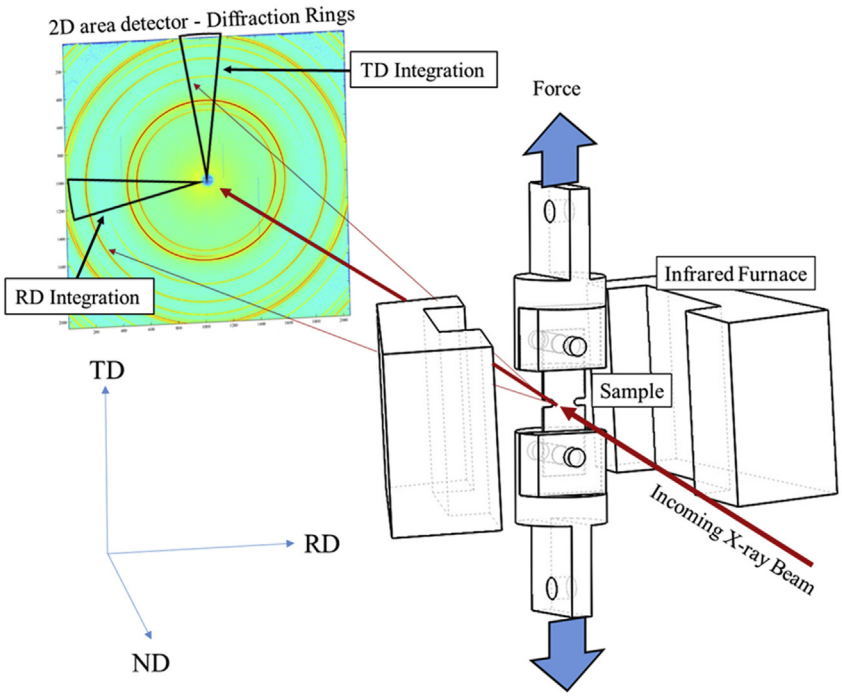

Fig. 6. Schematics of an example setup for in situ diffraction study using synchrotron radiation.

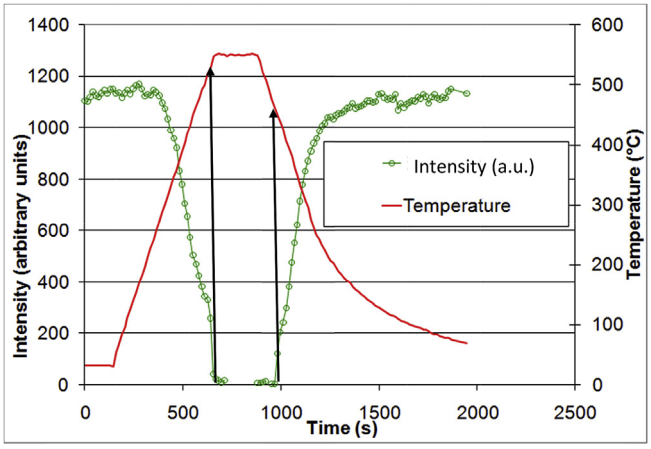

Fig. 7. Hydride diffracted intensity versus time examined with synchrotron radiation in a sample containing 530 wppm H plotted along with the temperature schedule used. Arrows indicate the end of dissolution and start of precipitation.

hydride particles that are composed of many nanoscale hydrides arranged in a "deck of cards" configuration within a single crystal, as shown schematically in Fig. 10. As shown schematically in the figure, in the absence of stress, the nanoscale hydrides have been reported to arrange themselves such that the mesoscale hydrides have an overall orientation of approximately 14.7° [81]. Although this value has been widely quoted and reported in the literature, the evidence from micrographs such as Fig. 9 indicate that the macroscale grouping of the hydrides is essentially horizontal, i.e., perpendicular to the normal direction of the sheet or the radial direction of the tube.

Even without any imposed temperature or stress gradients, it has long been recognized that the texture of zirconium alloys has a strong impact on the orientation of precipitated hydrides [64]. The common crystallographic textures seen in fabricated Zr alloys have the hcp basal poles preferentially oriented close to the normal or radial direction. Thus, the nanoscale hydrides form with the disc normals close to the radial or normal direction. The mesoscale hydrides form perpendicular to the radial direction and are designated as *in-plane or circumferential*. These mesoscale hydrides, often referred to as platelets, tend to form in long lines that can span more than 100 μm (see Fig. 8). There is some change in orientation from one grain to the next, however they maintain their linear shape, as shown in Fig. 3, Fig. 8, Figs. 9 and 11 and Fig. 29. It is unclear what causes the hydrides to form these long lines, as any crystallographic driving force would work to modify the hydride orientation when crossing grain boundaries.

Table 1
Crystal structure of delta and gamma zirconium hydrides" [45]

	composition	Crystal structure	Lattice parameter (nm)
Delta hydride	$ZrH_{1.66}$	fcc	0.478
Gamma hydride	ZrH	fct	a = 0.4596, c = 0.4969

4.2. Precipitation under stress

When cooled under a sufficiently high applied deviatoric tensile stress, dissolved hydrogen can precipitate as reoriented hydride

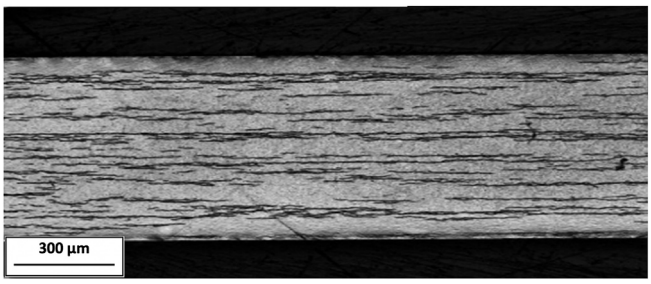

Fig. 8. Low magnification cross sectional micrograph of hydride precipitation in the absence of stress on a cold worked Zircaloy-4 sheet.

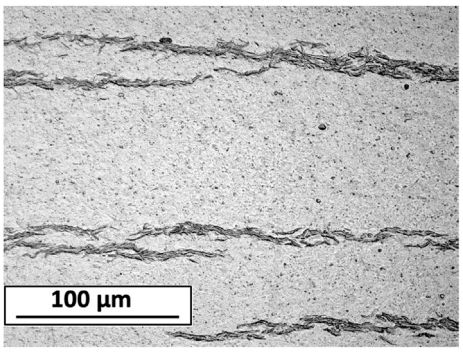

Fig. 9. High magnification micrograph showing a cross section of hydrided Zircaloy-4 [76].

needed for hydride reorientation.

The tensile stress that needs to be applied to the sample to achieve hydride reorientation during cooling is the threshold stress. The threshold stress for hydride reorientation has been determined by Desquines and co-workers [83] as

$$\sigma_{th}(MPa) = 110 + 65(1 - \exp(-[H]/65) \quad (5)$$

where σ_{th} is the threshold stress to cause complete reorientation of the hydrides and *[H]* is the hydrogen concentration in wppm.[1]

More recently the effect of stress state on the critical stress for hydride reorientation has been shown [76]. For a given principal stress, the presence of a secondary stress significantly decreases the stress required for hydride reorientation during precipitation under stress. Fig. 13 shows the threshold stress as a function of stress

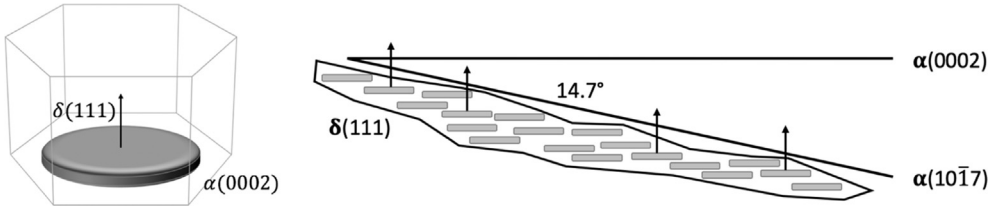

Fig. 10. Schematic diagrams, where the left image shows the nanoscale delta hydride disc and the right shows how nanoscale hydrides may aggregate into a mesoscale hydride.

platelets with their normals parallel to the applied stress [82]. Because the applied stress is often in the hoop direction, the hydride platelets then precipitate in the perpendicular direction to their normal circumferential orientation. These are called *radial* hydrides. Clearly given the brittle nature of hydrides, the radial or out of plane hydrides are much more likely than circumferential hydrides to promote the propagation of a crack in the radial or normal direction.

An example of the effect of stress on hydride orientation is shown in Fig. 11 which shows the orientation of hydrides in a tube stressed in bending. The inner part of the tube is under tensile hoop stress, so the hydride platelets are essentially radial whereas the outer part of the tube is in compression and so the hydrides precipitate as platelets in the circumferential direction.

Fig. 12 shows hydrides formed when submitted to stress during precipitation. The sample is tapered so that the stress changes within the gauge length. The threshold stress can be determined by matching the location of the reoriented hydrides with the calculated stress. In this case it is clear that a stress above 155 MPa is

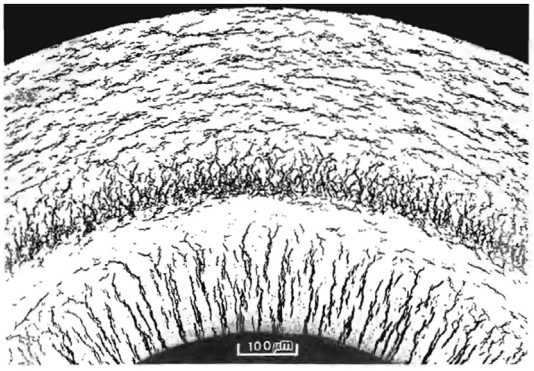

Fig. 11. Orientation of hydrides in a stressed tube in which stress is varying in tube thickness (courtesy C. Coleman, AECL).

biaxiality in the gauge section. As the stress biaxiality changes from uniaxial tension to equal biaxial tension the threshold stress decreases by half.

The precipitation of the hydrides under stress has the potential to lead to a slow-cracking mechanism, termed Delayed Hydride Cracking (DHC) [85–87]. This process is most commonly initiated at a stress concentration which, as noted above, causes the diffusion of hydrogen towards the high tensile hydrostatic stress. This leads to the precipitation of hydride platelets, following the crystallographic relationship discussed above, but with an orientation controlled by the stress field. Specifically, the hydride grows with its normal parallel to the maximum stress at the flaw as shown in Fig. 14. Under suitable conditions, this hydride or hydrided region will then fracture, leading to an extension of the flaw. The fracture will arrest in the zirconium matrix, which now becomes the location of a new stress concentration, and the process can repeat. Thus the flaw can extend in a repetitive process of hydride formation and fracture, where the timescale of the process is controlled largely by the diffusion of hydrogen and growth of precipitate. The phenomenon can occur (albeit slowly) even at room temperature [44].

At high magnification the hydride morphology is different for reoriented hydrides than for in plane hydrides. Fig. 15 shows that the reoriented hydrides appear at low magnification to be single particles, but at high magnification they appear to be horizontal segments which are stacked up vertically.

4.3. Thermomechanical cycling effects on hydride morphology

As discussed above, applied stress can cause hydrides to precipitate oriented in the radial direction rather than circumferentially. Experiments have also shown that when a single sample undergoes a number of thermal cycles, with precipitation always under an applied load, the fraction of radial versus circumferential hydrides increases as the number of cycles increases. Moreover, as

[1] In this case the cooling rate was between 0.5 and 5 °C/min.

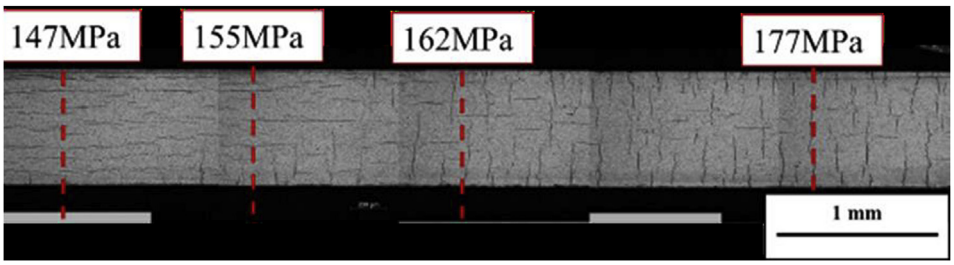

Fig. 12. Tapered sample of hydrided Zircaloy 4 showing different sections with varying stress and resulting hydride reorientation at a critical stress level [76].

the number of cycles increases, hydride particles tend to precipitate closer and closer to each other, increasing the connectivity of the hydrides, as shown in Fig. 16 Various researchers have demonstrated similar effects of thermal cycling, indicating that hydride-hydride interactions are important during hydride precipitation [70].

A memory effect has been noted in hydride precipitation when the temperature is raised sufficiently to dissolve the hydrides. The strains that form around the nanoscale hydrides are large enough to induce plastic deformation, emitting dislocations as shown in Fig. 17. As the precipitates dissolve at elevated temperature, the dislocations remain. When the temperature is subsequently decreased and precipitation commences, these dislocations could act as heterogeneous nucleation sites that causes the hydrides to form closer together [89].

The morphology of the mesoscale hydrides depends on the cooling rate, applied stress, and the history of the material. The radial hydride fraction (RHF), defined as the fraction of hydrides oriented radially over all the hydrides present in the microstructure [91,92], has emerged as a means of quantifying the hydride morphology. However it cannot capture the change in the spatial correlation, and in fact reduced spacing, of the hydrides that results from thermal cycling. Thus, another metric related to the connectivity or closeness of the hydrides is also needed to fully define the hydride morphology [57].

5. Modeling hydride precipitation and dissolution

Hydrides in the nuclear fuel cladding can have a significant impact on the mechanical behavior and ductility of the cladding. Thus, fuel performance codes require material models to predict hydrogen diffusion and hydride formation throughout the cladding as a function of the cladding temperature and stress fields. These models should predict not only the volume fraction of hydrides but also their morphology since the crack propagation through the cladding may be significantly impacted by the morphology. However, predicting the morphology of the mesoscale hydrides is a multiscale problem that requires critical insights on the formation of the hydride morphology from experiments at length-scales from nano-to micro-scale as well as from atomic and mesoscale modeling and simulation.

5.1. Modeling cladding hydrides in fuel performance analysis

Models for hydrogen migration and hydride precipitation and dissolution in the cladding need to be considered in fuel performance codes so that they can be included in the thermo-mechanic analysis of the fuel rod the effect of hydrides on the mechanical behavior and the consequent propensity for the cladding to crack. An example is the development of a modeling capability for hydrogen behavior in zirconium alloy claddings in the fuel performance code BISON [40,42]. In the following, we provide a brief summary of this capability as an example of hydrogen behavior modeling coupled to engineering fuel rod analysis. For more details, the reader is referred to the related publications [40,42].

The model in BISON computes (i) hydrogen generation and pickup at the outer cladding surface, which provides the flux boundary condition for hydrogen migration, (ii) hydrogen migration in the cladding, (iii) hydride precipitation and dissolution. In the model, hydrogen generation is computed as proportional to the

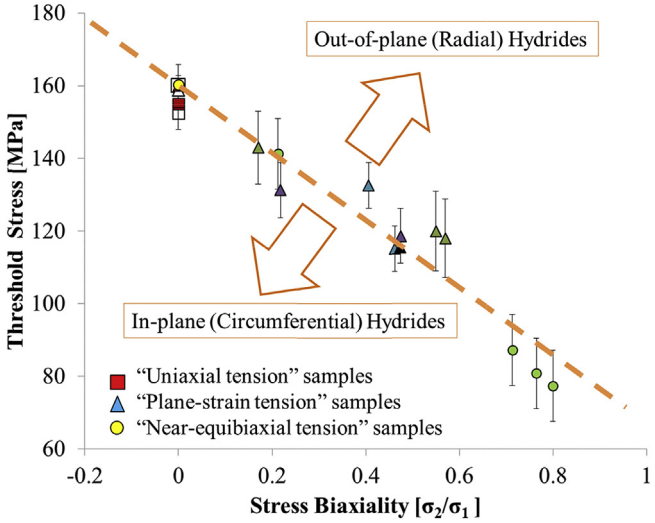

Fig. 13. Threshold principal stress (σ_1) for hydride reorientation during cooling for a sample containing about 200 wppm H as a function of stress biaxiality [84].

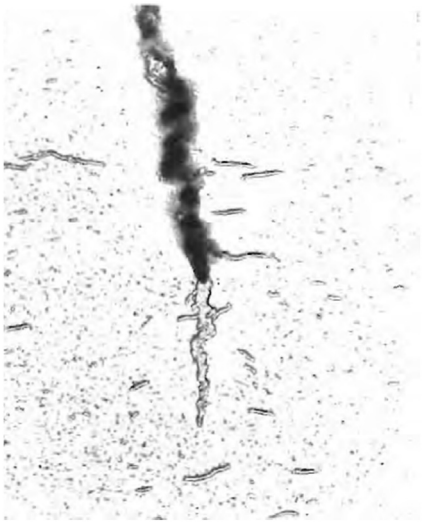

Fig. 14. Preferential Hydride precipitation at a crack tip (picture courtesy D. Rogers, AECL).

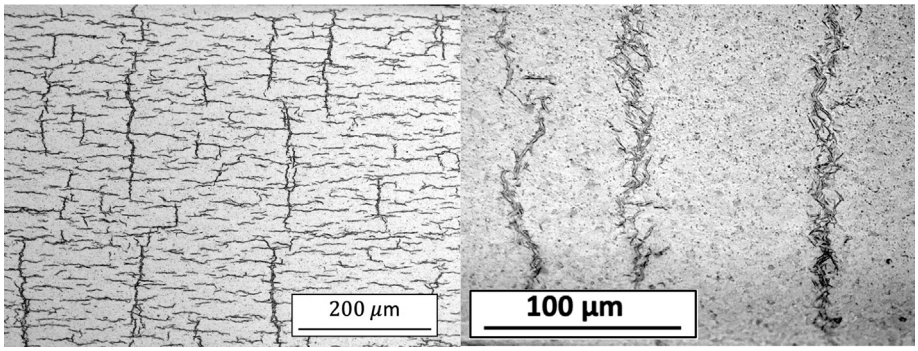

Fig. 15. (a) Cross sectional micrograph showing hydrided samples in which hydrides have been partly reoriented; (b) high magnification of reoriented hydrides [84].

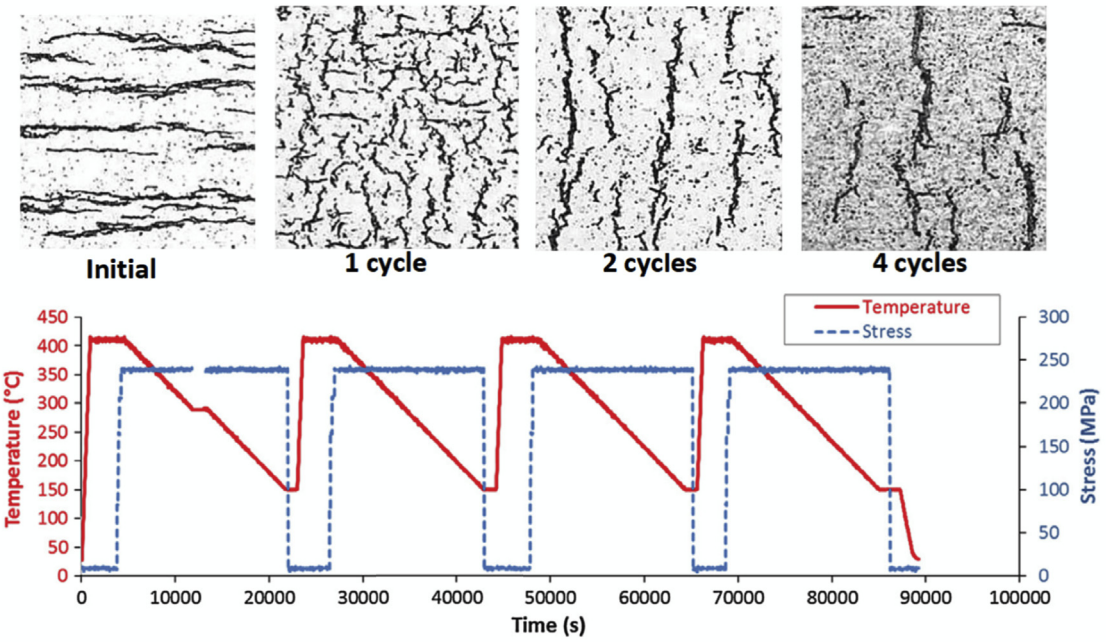

Fig. 16. Micrographs showing the reorientation of hydrides after several cycles in cold worked stress released Zircaloy-4 samples with 192 wt ppm of hydrogen cooled under 230 MPa applied stress with a cooling rate of 1 °C/min. The domain size is 200 μm^2 [88]. The micrograph on the left corresponds to the microstructure before the thermo-mechanical treatment described in the diagram, while the other micrographs corresponds to the microstructure after various cycles.

growth rate of the outer cladding oxide layer, which is consistent with hydrogen being generated during the waterside corrosion reaction of the zirconium alloy cladding. Oxide growth is calculated with the EPRI/KWU/CE model [93]. For simplicity, a constant hydrogen pickup fraction (Section 2) is used. Migration of hydrogen in solid solution is calculated considering both Fickian and Soret diffusion according to Eq. (3), using the values for the diffusion coefficient D_H and the heat of transport Q^*, but neglecting the flux from stress gradients. Hydride precipitation is computed using a rate equation of the form [94].

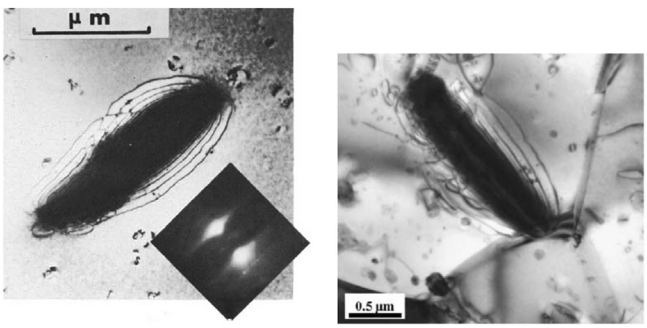

Fig. 17. TEM micrographs of nanoscale hydride discs that are surrounded by emitted dislocation lines, where the left image shows intragranular hydride in a Zircaloy-2 foil [90] and the right image shows a hydride adjacent to a grain boundary [80,89].

$$\frac{dC_{SS}}{dt} = -K_p\left(C_{SS} - TSS_p\right) \tag{6}$$

where $\frac{dC_{SS}}{dt}$ governs the rate of decrease of the hydrogen in solid solution, $C_{SS,}$ due to precipitation and K_p is a rate coefficient. The expression for the rate coefficient for precipitation as a function of the temperature from Ref. [39]is used.

Relative to the rate of precipitation, the rate of dissolution is assumed to be so high that equilibrium is maintained, and therefore $C_{SS} \approx TSS_d$ during dissolution. The Arrhenius relations for TSS_p and TSS_d as a function of the temperature from Ref. [95] are used in the model.

To compute the solution of the differential equations governing hydrogen behavior coupled to thermo-mechanics, BISON uses the Jacobian-free Newton-Krylov method in the MOOSE finite-element framework [96]. BISON has been applied to fuel rod lifecycle simulations to track the evolution of dissolved hydrogen and precipitated hydrides in the cladding [23]. Fig. 18 shows an example of results for the distributions of fuel and cladding temperature, and hydrogen in the cladding, for a 2D fuel rod analysis near the end of a 3.2-year steady-state irradiation under typical PWR conditions. The results demonstrate the higher hydrogen concentration near the outer surface of the cladding, which corresponds to the hydride rim formation, and the preferential redistribution of hydrogen into the regions adjacent to the inter-pellet gaps. The code was benchmarked in Ref. [97] by comparing the results to a nuclear fuel rod post irradiation experiment.

5.2. Atomic scale modeling of zirconium hydrides

Atomic scale modeling has been used to gain insights into the zirconium hydride system. These techniques, such as Density Function Theory (DFT) and Molecular Dynamics (MD), are based on the description of interatomic interactions, and they are limited to the study of a few hundreds of atoms at most for DFT, and as large as a few millions for MD. They can be employed to provide information about hydrogen diffusion in zirconium, thermodynamic and elastic properties of hydrides, interfacial energies between alpha Zr and hydride phases, as well as some clues as to the formation path of hydrides during precipitation.

Zhang coupled DFT and accelerated kinetic Monte Carlo simulations to derive the expression of the diffusion coefficient of hydrogen in alpha-Zr presented in equation (4) [52]. These values were validated against those by Kearns in Ref. [49], and extend the temperature range at which these values can be used. Domain also used DFT to provide insights into the behavior of hydrogen atoms in zirconium and in different hydride phases [98,99]. The study showed that hydrogen atoms tend to occupy tetrahedral sites of the hcp Zr, especially at low temperature. DFT and MD are also used to study the properties of hydride phases. The crystallography, as well as the thermodynamic and elastic properties of the zeta, gamma delta and eta hydrides phases were computed by Olsson [100] and Zhu [101,102], providing information about the elastic constants of the different phases, as well as their formation energies, their fracture behavior, and other aspects. Evaluating the stability of the different hydride phases provide important information about hydride precipitation. While Thuinet focused on the competition between zeta hydrides and gamma hydrides [103], Zhang studied the formation path of gamma hydrides using MD, which appears to undergo the following reaction: alpha (hcp) => zeta (hcp) => zeta (fct) gamma (fct) [50]. Hydrogen first nucleates as fully coherent hcp zeta hydrides, which then evolve into fct zeta hydrides before a phase transformation occurs to produce fct gamma hydrides.The gamma hydrides then become delta hydrides.

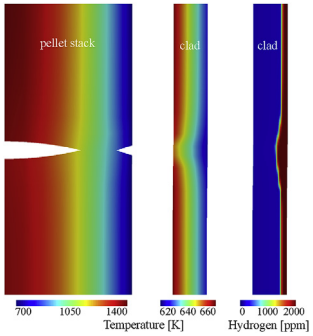

Fig. 18. From left to right: BISON prediction of temperature in the pellets, temperature in the cladding, and hydrogen concentration in the cladding near the end of 108 s of steady-state irradiation at 25 kW/m. The hydride rim is thickest adjacent to the (relatively cold) inter-pellet gap. The cladding has been enlarged by 2 in the radial direction to show more detail. From Ref. [42].

In addition to studying hydrogen behavior and hydride stability, atomistic simulations can determine the values of the interfacial energies in different orientation between alpha-Zr and hydride phases, which remain mostly unknown. Valuable efforts have been made to determine the energy of the basal and prismatic interfaces between alpha-Zr and gamma hydrides in Ref. [104]. However, more work is necessary to provide much-needed information to mesoscale models about the interface between alpha-Zr and delta hydride phases.

Atomistic scale modeling thus provides crucial insights into zirconium hydrides that would be extremely challenging to obtain experimentally, which can then be used to model hydride behaviors at larger scales.

5.3. Phase field modeling of hydride precipitation

While atomic scale simulation provides important insights into the mechanisms behind hydrogen transport and hydride nucleation, these methods cannot reach sufficiently large length or time scales to model the growth of the nanoscale hydrides and the organization of the mesoscale hydrides. Thus, mesoscale methods are also needed to represent hydride behavior. Mesoscale methods represent material behavior at scales ranging from hundreds of nanometers to hundreds of microns. Various mesoscale methods exist for predicting material behavior, however only the phase field method has been applied to modeling the formation and growth of zirconium hydrides.

Phase field modeling is a method of choice for studying microstructure evolution at the mesoscale [105,106]. The phase field method describes material microstructure using continuous variables that have distinct values in different regions of the microstructure. For example, to model the behavior of a delta hydride within an alpha zirconium matrix, a phase variable would have a value of one within a hydride and zero within the alpha zirconium matrix. Another variable is used to model the hydrogen concentration, which is allowed to evolve towards its equilibrium value in each phase. These variables smoothly transition between values across interfaces, such that all interfaces have a finite width. The evolution of these variables is defined by solving partial differential equations that lead to the reduction of the total free energy of the system. Furthermore, a phase field model can incorporate several thermodynamic driving forces like the bulk and interfacial energies, elastic contributions, plastic deformations, and other driving forces. As a result, phase field modeling is a powerful and versatile numerical method to study arbitrary complex microstructures of multi-physics systems like zirconium hydrides [15].

Phenomenological phase field models have been used to study the microstructure evolution of several hydride phases. Thuinet studied the evolution of the microstructure of zeta hydrides [107]. Significant contributions have been made by Chen, Ma, Shi and other authors on the effect of grain structure [108,109], the presence of other hydrides [110] or a crack tip or a notch [111,112], and applied stress [113] on the morphology of gamma hydrides [114,115], as shown in Fig. 19.

However, while phenomenological models provide valuable information on hydride microstructure evolution, they allow only qualitative comparison with experimental observations. Recent efforts have been made to develop quantitative phase field models

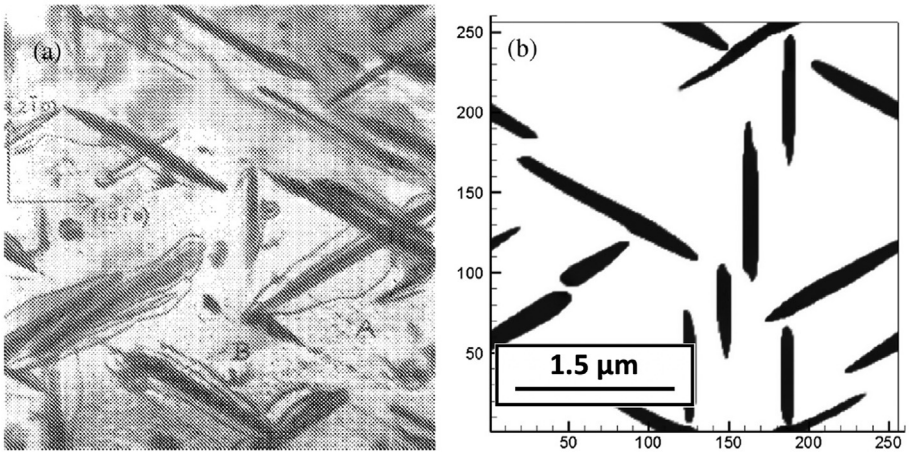

Fig. 19. Comparison of (a) TEM observations by Bailey [116] with (b) simulation results by Shi and Xiao [114].

by incorporating CALPHAD (Computer Coupling of Phase Diagrams and Thermochemistry) based free energies to the model. Jokisaari published a method to incorporate free energies of mixing into a phase field model for the alpha Zr/delta ZrH system [117], and Bair recently developed a phase field model for the alpha Zr/zeta ZrH/gamma ZrH/delta ZrH system using the free energies of formation of the different phases [118].

Despite the stochastic nature of nucleation processes, nucleation can be introduced into the phase field method by using a Langevin noise method [113] or an explicit nucleation method [119–125]. Both these methods have been used in phase field modeling of zirconium hydrides, in particular for the study of the gamma phase [113] and the delta phase [123].

Although the evolution of zirconium hydride microstructure has been studied extensively using phase field models, modeling efforts of the reorientation of delta hydrides under applied stress are still ongoing. Recent works include the contributions from Bair [126] and from Radhakrishnan [127], in which they both determine the magnitude of the applied strain needed to observe reorientation of a single nanoscale hydride disc. They both found that the minimum applied strains required for reorientating a single nanoscale hydride is extremely high, on the order of 0.01 (equivalent of a tensile stress of 894 MPa) [118,126,127] which is more than ten times higher than the 85 MPa observed in experiments needed to reorient 40% of mesoscale hydrides [88].

While the phase field method has the potential to provide critical insights into the impact of cooling rates, applied stress, and thermal cycling on phase field morphology, this potential has yet to be realized. The primary reason for this is the large difference in length-scales between hydrides within a grain and mesoscale hydrides that span many grains. The stacking and growth of the nanoscale hydrides must influence the mesoscale morphology, and thus the nanoscale hydrides cannot be ignored. As described above, the phase field method uses interfaces with a finite width, and a spatial mesh resolution is needed to solve the partial differential equations that is roughly one third of the width of the interface. If it is assumed that a nanoscale hydride has an initial thickness of 20 nm, then the interface width would need to be around 6 nm and the mesh resolution would need to be around 2 nm. However, at least 100 μm of material is needed to reasonably represent a mesoscale hydride, therefore on the order of 10^9 elements would be needed to represent that amount of material in 2D and 10^{14} in 3D. This number of elements could be reduced using mesh adaptivity, possibly to 10^8 elements in 2D and 10^{12} in 3D. Such a computation would be very large in 2D, requiring hundreds of processors on a computer cluster, and would be nearly impossible in 3D.

This issue with resolving the nanoscale hydrides implies that there may be another scale of simulations needed between those that resolve the nanoscale hydrides and the macroscale models needed for fuel performance codes. Microscale simulations could

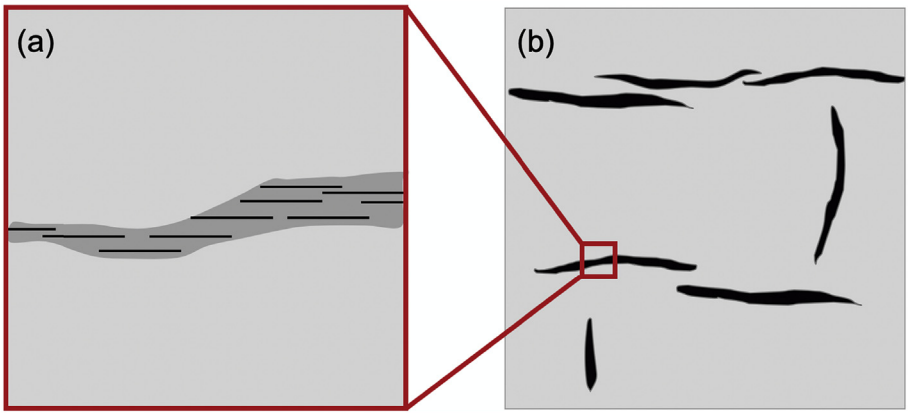

Fig. 20. Illustration of the different hydride scales. (a) shows the nanoscale hydrides. The domain size is of the order of hundreds of nanometers to a few micrometers square. (b) shows the mesoscale hydrides. The domain size is about hundreds of micrometers square. The two scales require different phase field models to have both the appropriate resolution of the nanoscale hydrides and gain information on hydride precipitation at the mesoscale.

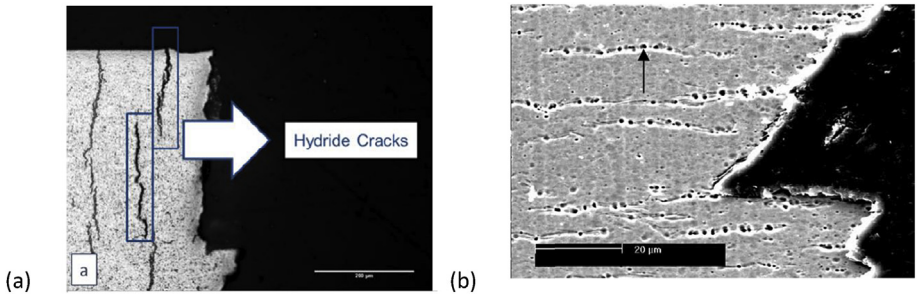

Fig. 21. Light micrographs showing (a) radial hydride particles initiating cracks while in (b) circumferential hydrides initiate strain-induced voids, resulting in damage accumulation failure. as opposed to fracture due to crack initiation and growth. 1.

be carried out that resolve tens to hundreds of the nanoscale hydrides to understand their behavior under applied loads, across many grain boundaries, and more. This information could then be used to develop a new model to represent the mesoscale hydrides without resolving the individual nanoscale hydrides. Such a model would not require the small resolution discussed above and therefore could be used to predict the hydride morphology in areas that are hundreds of microns across. The results of this model could then be used to investigate the impact of various conditions on the hydride morphology, providing the information needed to develop the macroscale model (see Fig. 20).

6. Mechanical properties

As mentioned above, the precipitation of hydrides has a significant impact on zirconium alloy cladding ductility and failure [128–132]. While uniformly distributed circumferential hydrides can affect the ductility of zirconium alloy cladding only at high hydrogen concentrations, certain hydride configurations can cause dramatic decreases in the fracture resistance even at low concentrations. In particular, the failure processes at low temperatures of hydrided cladding are quite different when circumferential and radial hydrides are present. As shown in Fig. 21a, radial hydride particles can initiate long cracks under load, and as a result, cladding failure at low temperatures when radial hydrides are present is often characterized by brittle fracture controlled by crack nucleation and a crack growth instability governed by the fracture toughness of the hydride matrix. In contrast, low temperature deformation of cladding with circumferential hydrides results in voids forming along the hydrides (Fig. 21b) leading to a damage accumulation type ductile fracture, such as analyzed in ref's [131–133]. For mixed microstructures, the failure process can be a complex combination of these two types of failure in which the fracture path can be quite tortuous.

Mechanical tests conducted on hydrided Zircaloy also show an influence of hydride distribution on overall cladding ductility. In particular, the presence of "unfavorable" hydride features such as hydride rims [134] or hydride blisters [18,135] can alter the cladding failure from ductile failure to "brittle-like" fracture through the initiation of cracks at hydrides. In the case of a hydride rim or hydride blisters, experiments show that as the thickness of a hydride blister or rim *increases*, the failure strain *decreases* as the hydrides crack near the yielding of matrix and subsequently cause failure of the uncracked ligament either by plastic deformation localization or near-brittle crack growth [18,134]. The susceptibility to brittle fracture is especially pronounced for thick hydride rims and/or if the uncracked ligament has a low fracture toughness, such as if radial hydrides are present [136].

In the absence of crack growth (such as at elevated temperatures), ductile failure can occur at small far-field strains due to deformation localization. In this case, the early cracking of a hydride rim or blister reduces the load-bearing cross section area, leading to a "localized necking" instability to develop in the location [137,138]. As a result, the presence of hydride rims [126] or blisters [18,135] may reduce cladding ductility even in the absence of crack growth. We note that this analysis provides an upper bound for the failure strain, while the presence of a sharp crack can cause brittle failure to intervene at small strains and at stresses at/or below the yield stress.

Modeling of hydrided material failure has used mean field approaches such as the calculation of the strain energy density as a primary parameter for failure [139,140]. Such models however do not take into account the localization of failure such occur when a hydride rim fails early during deformation and which can govern through-wall fracture [137].

Although much work has been performed in this area, the problem of determining failure limits from crack propagation is complex and has yet to be resolved. One important issue is that the matrix yield stress must be sufficiently high in order that the level of strain concentration at the hydride can elevate the local stresses to cause hydride cracking. As a result, hydride fracture can occur at low temperature even though the hydride is believed to be stronger than the matrix. This is normally true in cold-worked stress-relieved material or irradiated material, to a greater degree than in recrystallized material [141,142]. There is also evidence that the tensile stress to fracture hydrides increases with hydride length for short hydrides but is insensitive when hydride length exceeds about 25 μm [143]. We note that the most likely stress state to be exerted onto Zircaloy cladding is essentially that of a bi-axially loaded thin walled pressure vessel, in which the largest stress is in the azimuthal, or hoop direction, and results from the pressure differential with the primary coolant by fission gas release, or pellet-cladding mechanical interaction. For crack-growth dominated failure, the hoop stress (i.e., the maximum principal stress) is then the critical stress.

The presence of radial hydrides promotes *both* crack initiation and crack growth *if* the temperature is sufficiently low for the hydrides to form cracks. As shown for the behavior of ring compression tests in Fig. 22 [144–146], the presence of radial hydrides causes an abrupt transition from ductile to brittle behavior upon a small decrease in temperature. For similar hydrogen contents, the ductile-to-brittle transition temperature (DBTT) is much higher when radial hydrides are present when compared to cladding with only circumferential hydrides. The radial hydride-induced brittle behavior shown in Fig. 22 depends on the initiation of cracks at the radial hydrides (see Fig. 21a), so that if no cracks occur, neither does brittle fracture. Above the DBTT, as matrix deformation occurs, the radial hydrides appear ductile and deform, and no cracks are present [147]. Fig. 23 shows that even in the case of circumferential hydrides, there is a strong effect of test temperature such that

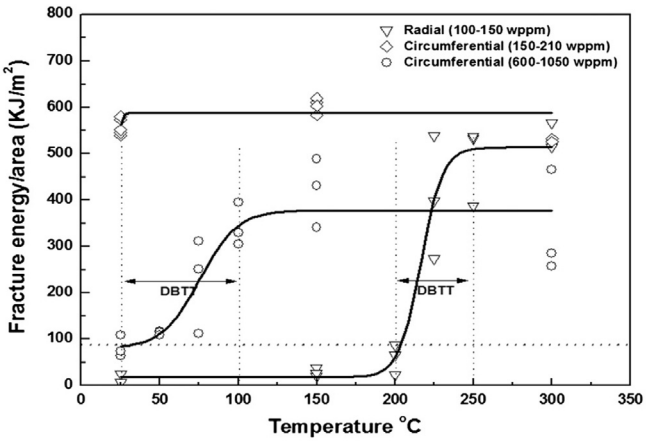

Fig. 22. Fracture Energy versus testing temperature for radial and circumferential hydrides in Zircaloy tested with ring compression tests [144].

hydrides crack and form elongated voids ahead of the crack at low temperatures but appear to be ductile at high temperatures. Unlike radial hydride "damage", the circumferential hydride damage at low temperatures is in the form of elongated voids (Fig. 21b) which undergo strain-induced growth and coalescence such that the cladding exhibits ductility even at low temperatures (unless the hydride content is exceedingly high—as in the case of a hydride rim).

Crack initiation at radial hydrides is quite sensitive to testing temperature with the ductile to brittle transition occurring over a relatively small range of temperatures (approximately 50 °C). The deformation behavior of the ductile zirconium alloy matrix should undergo comparatively small changes over such a small temperature range. Thus, if hydride fracture is caused by strain-induced incompatibility stresses between the radial hydride particles and the deforming zirconium alloy matrix, we might speculate that hydride fracture behavior must change rapidly near the DBTT. The ductile to brittle temperature reported in Ref. [133] is for cladding with 100 wt ppm H and is in the range of 200°–250 °C; thus, some degree of hydride dissolution is expected. However, the extent of dissolution (perhaps 30% according to Fig. 4) does not appear to be able to reduce the approx. 150 μm hydrides in these claddings to the 25 μm ductile transition length suggested in Ref. [143]. Reducing the hydride size to a "ductile" length is even more difficult for the case of Zircaloy-4 with 200 wt ppm hydrogen that shows a DBTT at 125°–150 °C when the hydrides lengths range to 300 μm; see the small extent of hydride dissolution predicted by Fig. 4. In summary, although hydride ductility appears to change rapidly near the DBTT, this change does not appear top be the cause of the DBTT.

Once a crack initiates at a macroscopic radial hydride, crack growth is sensitive to both the length of the initiated crack *and* to the three-dimensional radial hydride microstructure, especially radial hydride content as well as the connectivity or continuity of the hydrides. The fraction of hydrides that are radial relative to circumferential can be quantified by the radial hydride fraction:

$$RHF = \frac{0.5 \cdot \sum_i L_i^{mixed} + \sum_j L_j^{out-of-plane}}{L_{total}} \times 100 \quad (7)$$

where the $L_j^{out-of-plane}$ is the length of radial (out of plane) hydrides in a given micrograph L_j^{mixed} is the length of hydride that are in between radial and circumferential while L_{total} is the total hydride length.

The presence of radial hydride particles has a direct influence on crack propagation, whereas circumferential hydrides can help only to a lesser degree. However, the impact of hydrides on crack propagation is related to more than just their orientation; the specific hydride morphology also has a strong influence on the failure strain, as shown in Fig. 24. It is possible to define the hydride connectivity as the remaining ligament after the easiest path through the cladding is identified within a length λ. On the leftmost example three vertical hydrides cover about 57% of the cladding thickness. As deformation starts, these hydrides will crack at very small strains so that they will then be joined by 45-degree ductile slip in between (bottom). In the middle example the coverage is similar (50%) but a much bigger deformation band would have to develop, making this an unlikely site for failure. This is because the rightmost hydride particle is beyond a distance of λ. On the right most example, the coverage within the relevant range of λ is even higher, but now with a combination of vertical and in-plane hydrides for a coverage of about 70%. When load is applied, the hydrides fail early during deformation (at a small strain) so that failure of the component now hinges on the failure of the remaining ligaments) so that a crack can propagate through the thickness of the material.

As noted earlier, the mechanical strength and ductility of zirconium-based alloys can be significantly compromised by the formation of hydrides because they have lower fracture strength than pure zirconium, and they can be sites of fracture initiation and embrittlement, which subsequently leads to cladding rupture and failure [149]. Predicting the fracture mechanisms of these matrix-hydride composite materials is difficult because the heterogeneous microstructure of these Zircaloys can have a significant effect

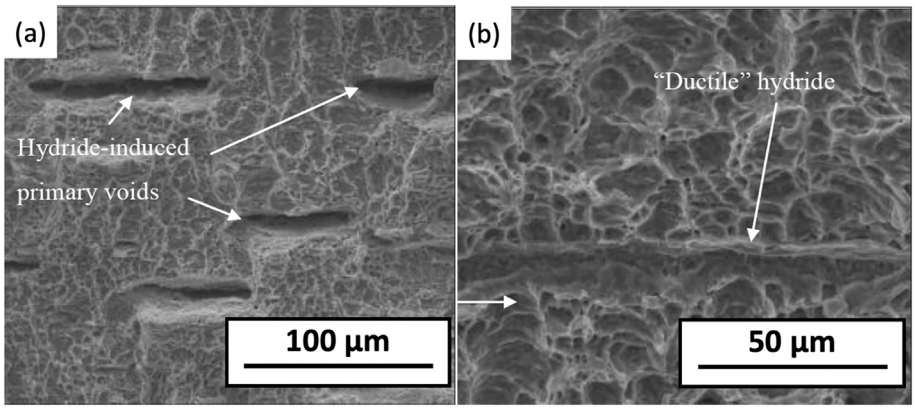

Fig. 23. Scanning electron fractographs of Zircaloy-4 fracture toughness samples with circumferential hydrides tested at (a) room temperature and (b) 300 °C [148].

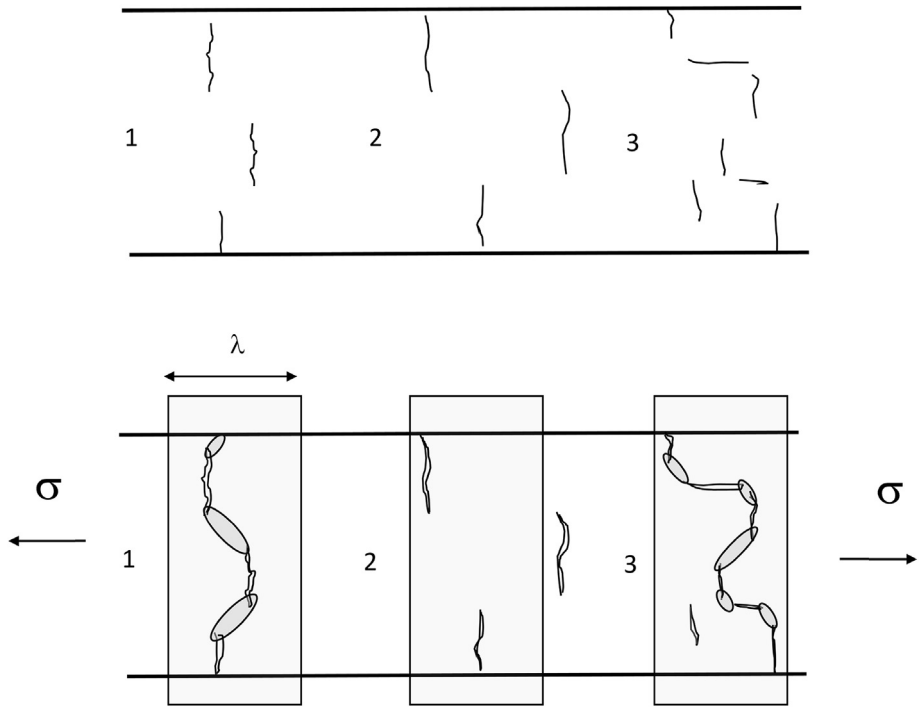

Fig. 24. Illustration of hydride connectivity. (a) three different hydride configurations, (b) as deformation happens, hydride particles crack after small strains and are then linked.

on failure behavior, and these heterogeneities can severely limit the use of phenomenological or macroscopic fracture approaches. These physical heterogeneities, which span different spatial scales ranging from the nano to the micro include local and internal stresses and strain incompatibilities between the matrix and hydride interphases, semi-coherent interfaces, grain-boundary defects, grain morphologies and orientations, dislocation-density accumulations at matrix-hydride interfaces.

Due to this complex relationship between heterogeneities and cladding fracture mechanisms, three-dimensional microstructurally-based fracture approaches at different physical scales are essential and should be integrated with strain-based continuum models and experiments to obtain validated predictions of hydride crack nucleation, hydride connectivity, and overall rupture for different populations and orientations of hydrides on a physically relevant continuum scale, such that fracture measures for both hydride crack nucleation and propagation can be attained. Furthermore, a key feature of any fracture methodology, due to the differences in the hydride and matrix crystalline structures, would be distinguishing between hydride cracking and matrix cracking in these multi-phase aggregates.

To address some of these challenges, a nonlinear fracture methodology has been developed by Ref. [149] that is coupled to a three-dimensional dislocation-density crystal plasticity formulation, and it can be used to predict hydride cracking and linkage in terms of morphological and crystallographic characteristics, defects, and different interfaces related to different crystallographic interphases, grain boundaries, and hydride populations. It has been used to predict and understand intergranular and transgranular fracture nucleation and growth mechanisms along energetically favorable slip-planes, cleavage planes, and grain boundaries in Zircaloys subjected to different thermo-mechanical loading conditions and scenarios. The approach is tailored for hydride fracture, since it accounts for different hydride crystalline structures, such as δ (fcc) and ε (bcc) that have precipitated within the hcp Zircaloy matrix. The different hydride crystalline structures are physically represented by orientations relations (ORs) and misfit strains at the matrix-hydride interfaces. The fracture approach is based on a finite element (FE) overlap method that utilizes phantom nodes to nucleate failure surfaces once critical stresses are attained.

An example of this approach is shown in Fig. 25, which pertains to the normalized stress profile crack nucleation and propagation around δ hydrides. This approach provides a means of quantifying the impact of hydride fraction, orientation, and connectivity on the fracture.

Due to different thermo-mechanical loading conditions, hydrides can evolve from a circumferential to radial orientation. This reduces the overall strength of the cladding, since it provides an energetically favorable fracture path through the cladding wall. In zirconium alloys, precipitation of a hydride generally introduces internal stresses in the surrounding. Adopting a reasoning considering elasticity only, the stress induced by the hydride (i.e. by the

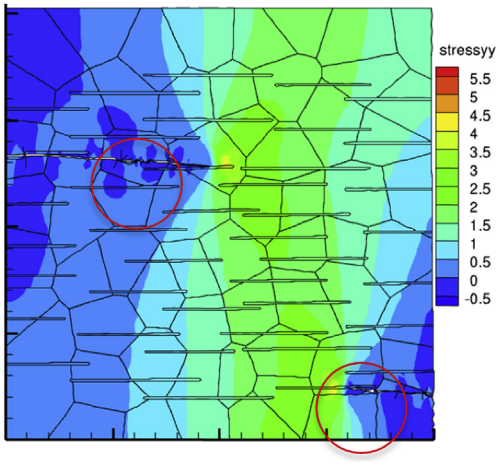

Fig. 25. Normalized normal stress distribution for nucleating cracks (circled areas) for a Zircaloy specimen with radial δ hydrides.

stress-free transformation strain resulting from the hydride formation) can easily reach 400 MPa. Clearly such high stresses could be relieved by the activation of plastic deformation mechanisms. Understanding the evolution and role of internal stresses on the formation, growth and arrangement of delta hydrides in Zircaloy is essential. Tummala and co-workers [150] have used Fast Fourier Transform (FFT) based discrete dislocation dynamics technique to quantify both internal stresses induced during the formation of a hydride and the relief of the internal stresses by dislocation nucleation from the hydride-matrix interface. Consistent with experimental observations (see Fig. 19), it is found that the dislocation emission from hydrides is thermodynamically possible. Fig. 26 shows an image of a predicted microstructure resulting from the relaxation of internal stresses near the hydride by the emission of dislocations on basal planes. Interestingly, as shown in Fig. 26b, it is found that the dislocations nucleated from the hydride-matrix interface could act as loci for the nucleation of new hydrides. Importantly, the study also suggests that the observed 'deck of card arrangement' of hydrides, shown in Fig. 10, in which hydrides line up at angles in the order of 14° and are spaced apart from one another could be a consequence of the dislocation nucleation mediated relaxation process studied in Ref. [150].

These microstructural scale fracture and internal stress predictions can then be used to inform large scale 3D elasto-plastic phenomenological FE analyses that can be utilized within DOE codes, such as Moose/BISON, to determine stress and strain evolution and localization of Zircaloys. More critically, these continuum stress and strain level predictions can serve as benchmarks for the microstructural and FFT-dislocation-dynamics analyses to delineate what microstructural effects, such as grain orientations and morphologies and texture, are dominant and affect continuum level stresses. This is essential for the determination of physically realistic fracture criteria that spans the microstructural to continuum scales. Physics-based material models for continuum level predictions of ceramic UO_2 fuels and Zircaloys have been incorporated [151] in codes, such as BISON. These models are based on irradiation induced clad creep and growth, clad corrosion, the hydrogen pickup and hydride precipitation in the clad, and the release and transport of fission produced gas. This architecture includes the ability to incorporate or develop material properties libraries and fuel behavior models for UO_2 fuel and zirconium alloy cladding commonly used in LWRs. These models consist of irradiation induced clad creep and growth, clad corrosion, the hydrogen pickup and hydride precipitation in the clad, and the release and transport of fission produced gas. An example of this approach, which is based on modeling efforts detailed in Ref. [151] is shown in Fig. 27, where the temperature distribution within the fuel and cladding is superimposed with a metallography image of a typical fuel pellet. These fuel performance simulations activities provide an understanding of how hydride precipitate distributions in the fuel cladding and the probability for cladding failure during fuel assembly storage and transportation behave at the structural or macroscopic scale level.

These interrelated approaches can provide a physically based framework that can be used to account for hydride reorientations, dislocation-densities, inelastic strains, and local stress fields, such that mechanical behavior and fracture nucleation on the submicron level and hydride cracking can be scaled to the structural level for different hydride populations and orientations. More significantly, it has the potential for the development of validated fracture criteria that spans the microstructural scale to the continuum scale for hydride cracking, connectivity and overall rupture.

7. Research needs

It is clear from the preceding that zirconium hydride formation during precipitation is a complex phenomenon involving multifaceted physical processes and which can strongly affect cladding mechanical properties. Although research has been done which has identified important phenomena, several fundamental questions still require attention:

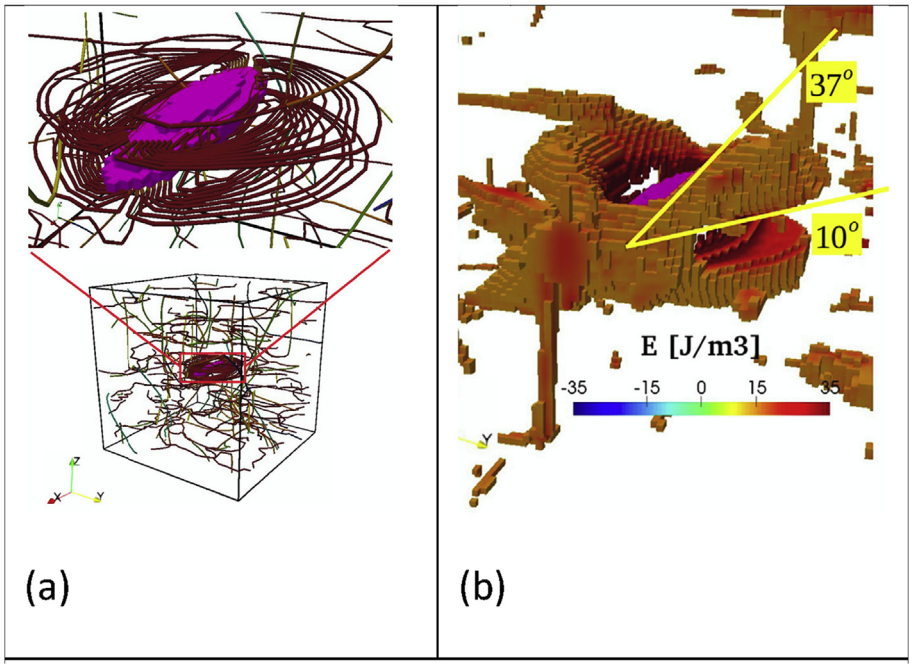

Fig. 26. (a) Close-up view of a single crystal containing a 375 nm × 91 nm ×37.5 nm hydride (in pink) in the presence of a dislocation network after relaxation by dislocation emission is permitted, (b) 3D map of potential for dissipating elastic strain energy by forming a new hydride around an existing hydride shown. Only regions in which hydride nucleation is thermodynamically possible are shown. (For interpretation of the references to colour in this figure legend, the reader is referred to the Web version of this article.)

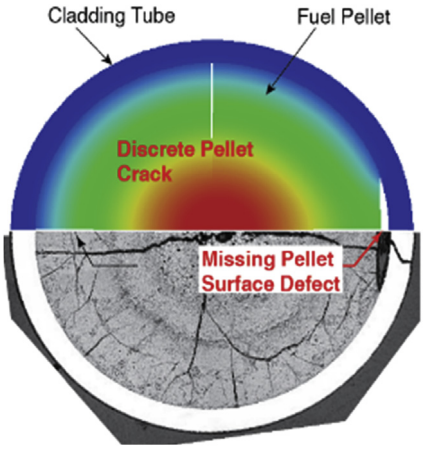

Fig. 27. 2D plot of the temperature distribution in a cross section including: the cladding, the cracked fuel pellet with missing pellet surface defect.

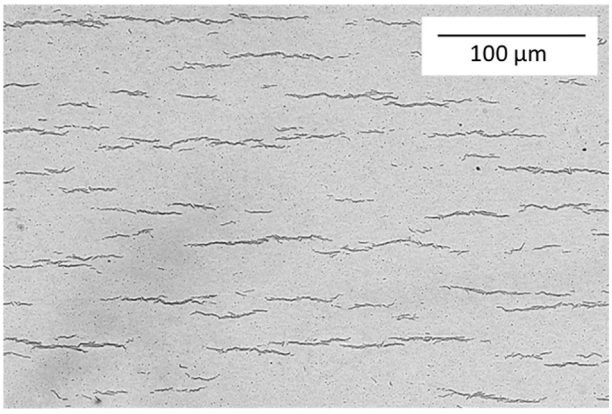

Fig. 29. Low magnification SEM micrograph of hydride microstructure in Zircaloy-4.

a) How do the mesoscale hydride microstructures form?

The principal problem to be understood is illustrated in Fig. 28. When observed in high magnification the hydrides look like individual segments, of the same order of the grain size and with slight mis-orientations relative to each other. This is consistent with the picture of hydrides having an orientation relationship with the matrix and changing slightly from grain to grain to maintain it, although this has not been explicitly verified.

More important is the fact that when seen in low magnification (Fig. 29) the hydrides extend over distances of the order of 100 μm, i.e. much longer than the grain size (about 1–2 μm for equiaxed grains in RX material) and almost perfectly aligned. This alignment is clearly governed by hydride-hydride interactions (such as in sympathetic nucleation) or by hydrogen-hydride interactions (anisotropic growth), with the effect, that hydrides tend to form in "bunches". The tendency of the hydride particles to align themselves during thermomechanical treatment is the crucial factor in the onset of material degradation. It is the size and orientation of these that is the most crucial to predicting hydride degradation of mechanical properties.

The problem can be posed graphically in the following way: Fig. 30 shows schematically the first hydride nucleus precipitated once TSSp is reached. This initial precipitation can obey the orientation relationship or could occur for example near a grain boundary. As further cooling occurs, additional hydrogen will precipitate. This additional precipitation could occur at various points in the material. It could occur near the edge of the existing hydride (position 1), slightly offset (position 2), on top of the hydride (position 3) or in a random position in the material (position 4). This is true both for nucleation of a new hydride or growth of an existing one. Clearly several macroscopic hydrides are formed a certain distance from each other so nucleation at 4 occurs. It is also clear that precipitation happens near position 1, possibly with a little offset (position 2). This causes the initial hydride to "elongate", with the continuation of this process eventually resulting in the microstructure seen in Fig. 29.

This elongation could be caused by the initial hydride particle growing preferentially in the horizontal direction or by the nucleation of a new particle (see two paths drawn in the Figure). In the first scenario, the hydride would grow into another grain, and thus would cease to maintain the orientation relationship with the matrix whereas in the second case new hydride nucleation would need to occur. One could then ask why the hydride growth is anisotropic and possibly the answer would be in the transformational strains or the hydride surface energies being anisotropic. In the second hypothesis, new hydride nucleation would need to occur preferentially near the hydride edges. This could be favored by the elastic strain field induced by hydride precipitation or by the presence of dislocations at the edge.

Regardless of the mechanism, the final result is Fig. 29, in which 100-μm long mesoscale hydrides form in a matrix where the grain size is much smaller. The fact that the mesoscale hydrides are more or less evenly spaced indicates that each cluster took their hydrogen atoms from "their" region, i.e. several hydride embryos are nucleated and grow horizontally.

b) What causes hydride reorientation? What is the role of stress?

Although the limits for hydride reorientation in terms of threshold stress have been established it is not clear why stress acts to reorient the hydrides. Returning to the schematic illustration

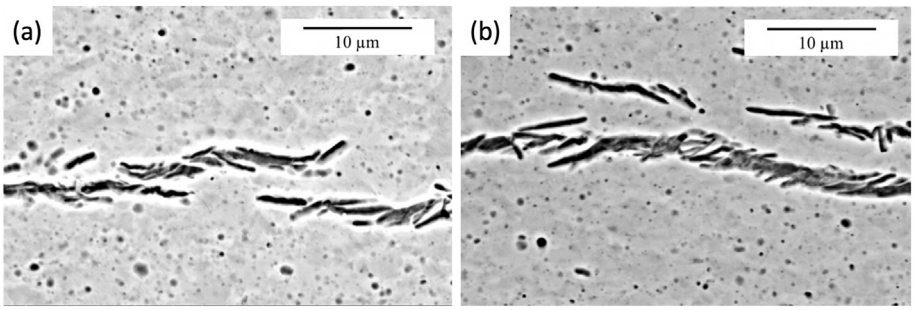

Fig. 28. High magnification SEM micrograph of hydride particles in Zircaloy-4.

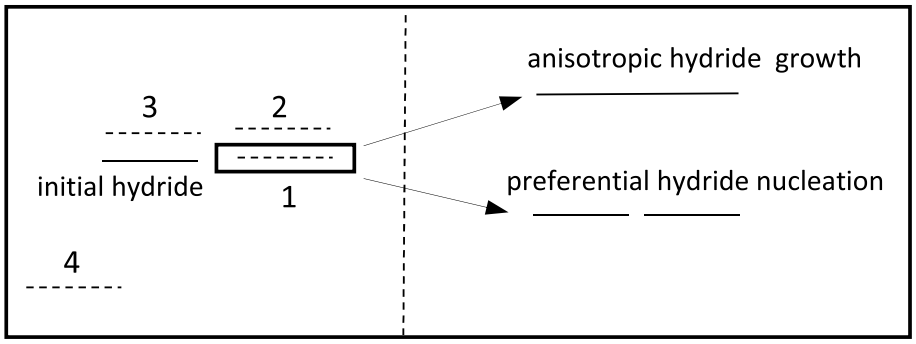

Fig. 30. Schematic processes for creation of hydride alignment.

shown in Fig. 30 when a tensile stress is applied during precipitation the next hydride particle to be formed would be on position 3 rather on position 1. The small hydrides would then stack vertically as in Fig. 15 b) and form mesoscale reoriented hydride microstructures.

We do not have a clear image of the hydride distribution in 3D, either for the circumferential or for the radial hydrides. It is possible that the circumferential hydrides seen in Fig. 29 have a platelet shape, but is also possible that they resemble a plate of beans, aligned in the same plane but formed of individual particles. The structure of the reoriented hydrides seen in Fig. 15 b may stretch in the direction perpendicular to the surface of the paper as stacked ribbons (or venetian blinds) or be constituted of a Jackson Pollock type collection of individual hydrides formed on the same plane. The presence of a collection of small individual hydride particles on the same plane would indicate *preferential nucleation* whereas the larger scale particles would indicate *preferential growth* as the cause of hydride alignment.

What is clear is that although the usual explanations for hydride alignment (orientation relationship/texture, grain boundary orientation) can contribute to the formation of the initial hydrides and thus the mesoscale microstructure, they cannot explain the formation of such long hydride microstructures as seen in Fig. 29 or Fig. 15 b as the matrix grain size is much smaller than the hydride size.

c) What causes the sudden change in ductility over a relatively narrow temperature range?

The temperature dependence of the mechanical response of the material is not well understood. When subjected to tensile testing, such hydrided materials tend to fail at small strains. The mechanical response of the composite material at various temperatures and thus the overall ductile to brittle transition of the hydrided component needs to be understood, especially its abrupt change within a small temperature range.

Temperature dependence of mechanical properties and fracture: in addition, the temperature dependence of the mechanical response of the material is not well understood. When subjected to tensile testing, such hydrided materials tend to fail at small strains. The mechanical response of the composite material at various temperatures and thus the overall ductile to brittle transition of the hydrided component needs to be understood through well-coordinated experimental testing and modeling, especially with respect to this abrupt change within a small temperature range.

d) How do these questions change for different alloys and potentially different microstructures?

This was not discussed in this review, but it is possible that different alloys show different hydriding behavior, independent of eventual differences in corrosion or hydrogen pickup, i.e. for the same hydrogen content. Two phase alloys such as the Canadian Zr2.5%Nb should be most different but differences in behavior between other Nb containing alloys and Zircaloy have also been observed.

8. Conclusion and perspectives

Hydrogen enters the nuclear fuel cladding as a result of waterside corrosion that happens in service. After hydrogen enters the material, hydrogen redistributes in the cladding tube in response to driving forces from concentration, temperature and stress gradients, which creates local increases in hydrogen concentration. Once the local hydrogen concentration exceeds the terminal solid solubility in the matrix, hydride particles can precipitate. This causes the ductility of the composite material (zirconium matrix with hydrides) to decrease relative to that of unhydrided material.

The local hydrogen concentration is governed by the overall hydrogen content of the material, the temperature schedule (highest temperature, hold time, cooling rate) and the presence of significant concentration, temperature and stress gradients in the material.

The failure probability of hydrided Zircaloy is governed not only by the overall hydrogen content but by (i) the local hydride content and local hydrogen concentration, (ii) the hydride orientation and overall mesoscale hydride microstructure, (iii) the stress state imposed on the cladding as well as the testing temperature. In turn the mesoscale hydride microstructure depends on complex issues such as the sympathetic nucleation of hydrides and the presence or not of applied stress during hydride nucleation and growth.

Such issues are being investigated using state of the art experimental and computational techniques to establish the limits at which the hydride microstructure created significantly affect cladding ductility.

Acknowledgments

This review was prepared in the context of the DOE NEUP Integrated Research Project IRP-17-13708 “Development of a Mechanistic Hydride Behavior Model for Spent Fuel Cladding Storage and Transportation”.

References

[1] R. Yang, O. Ozer, H. Rosenbaum, Current challenges and expectations of high performance fuel for the millennium, Light Water Reactor Fuel Performance Meeting, Park City, Utah, 2000.
[2] M. Griffiths, J. Nucl. Mater. 159 (1988) 190–218.

[3] W.J.S. Yang, R.P. Tucker, B. Cheng, R.B. Adamson, J. Nucl. Mater. 138 (1986) 185–195.
[4] A.T. Motta, C. Lemaignan, A ballistic mixing model for the amorphization of precipitates in zircaloy, J. Nucl. Mater. 195 (1992) 277–285.
[5] A.T. Motta, A. Couet, R.J. Comstock, Corrosion of zirconium alloys used for nuclear fuel cladding, Annu. Rev. Mater. Res. 45 (2015) 311–343.
[6] C. Lemaignan, A.T. Motta, Zirconium alloys in nuclear applications, B.R.T. Frost (Ed.), Materials Science and Technology, A Comprehensive Treatment, 10 B, VCH, New York, 1994, pp. 1–51.
[7] H.G. Rickover, L.D. Geiger, B. Lustman, History of the development of zirconium alloys for use in nuclear reactors, Energy Research and Development Administration, Div. of Naval Reactors, Washington, D.C, 1975, 21 Mar 1975. 84pp.
[8] G.P. Sabol, ZIRLO an alloy development success, 14th ASTM INternational Symposium on Zr in the Nuclear Industry, Stockholm, ASTM STP-1467, 2005, pp. 3–24.
[9] G.L. Garner, J.P. Mardon, Alloy M5 in action, Nucl. Eng. Int. 47 (2002) 36–37.
[10] S. Kass, Hydrogen pickup in various zirconium alloys during corrosion exposure in high-temperature water and steam, J. Electrochem. Soc. 107 (1960) 594–597.
[11] R.S. Daum, D.W. Bates, D.A. Koss, A.T. Motta, The influence of a hydrided layer on the fracture of Zircaloy-4 cladding tubes, International Conference on Hydrogen Effects on Material Behaviour and Corrosion Deformation Interactions, Sep 22-26 2002, Moran, WY, United States, 2003, pp. 249–258. BN - 0873395018.
[12] D.L. Douglass, The Metallurgy of Zirconium, International Atomic Energy Agency, Vienna, 1971.
[13] J.J. Kearns, Terminal solubility and partitioning of hydrogen in the alpha phase of zirconium, Zircaloy-2 and Zircaloy-4, J. Nucl. Mater. 22 (1967) 292–303, 1967/6.
[14] C.E. Ells, Hydride precipitates in zirconium alloys, J. Nucl. Mater. 28 (1968) 129–151.
[15] A.T. Motta, L.-Q. Chen, Hydride formation in zirconium alloys, J. Met. 64 (2012) 1403–1408.
[16] M. Blat, L. Legras, D. Noel, H. Amanrich, Contribution to a better understanding of the detrimental role of hydrogen on the corrosion rate of zircaloy-4 cladding materials, Twelfth International Symposium on Zr in the Nuclear Industry, Toronto, ASTM STP-1354, 2000, pp. 563–591.
[17] A.M. Garde, G.P. Smith, R.C. Pirek, Effects of hydride precipitate localization on the ductility of irradiated zircaloy-4, 11th International Symposium on Zr in the Nuclear Industry, Garmisch-Partenkirchen, Germany, ASTM STP-1295, 1996, pp. 407–430.
[18] O.N. Pierron, D.A. Koss, A.T. Motta, K.S. Chan, The influence of hydride blisters on the fracture of Zircaloy-4, J. Nucl. Mater. 322 (2003) 21–35.
[19] R.S. Daum, S. Majumdar, M.C. Billone, Mechanical properties of irradiated Zircaloy-4 for dry cask storage conditions and accidents, 2003 Nuclear Safety Research Conference, Washington, D.C, 2003, pp. 85–96.
[20] R.S. Daum, S. Majumdar, Y.Y. Liu, M.C. Billone, Radial-hydride embrittlement of high-burnup Zircaloy-4 fuel cladding, J. Nucl. Sci. Technol. 43 (2006) 1054–1067.
[21] S. Yagnik, R.B. Adamson, G. Kobylyansky, J.-H. Chen, D. Gilbon, S. Ishimoto, et al., Effect of alloying elements, cold work, and hydrogen on the irradiation-induced growth behavior of zirconium alloy variants, 18th International Symposium on Zirconium in the Nuclear Industry, May 15, 2016 - May 19, 2016, Hilton Head, SC, United States, ASTM STP-1597, 2018, pp. 748–795.
[22] J.C. Brachet, L. Portier, T. Forgeron, J. Hivroz, D. Hamon, T. Guilbert, et al., Influence of hydrogen content on the alpha/beta phase transformation temperatures and on the thermal-mechanical behavior of Zy-4, M4 (ZrSnFeV), and M5 (ZrNbO) alloys during the first phase of LOCA transient, Zirconium in the Nuclear Industry: Thirteenth International Symposium, ASTM STP-1423, 2002, pp. 673–701.
[23] A. Couet, A.T. Motta, R.J. Comstock, Hydrogen pickup measurements in zirconium alloys: relation to oxidation kinetics, J. Nucl. Mater. 451 (2014) 1–13.
[24] A. Couet, A.T. Motta, R.J. Comstock, Effect of alloying elements on hydrogen pickup in zirconium alloys, 17th International Symposium on Zirconium in the Nuclear Industry, Hyderabad, ASTM STP-1543, 2013, pp. 1–33.
[25] B. Cox, C. Roy, The Use of Tritium as a Tracer in Studies of Hydrogen Uptake by Zirconium Alloys, vol. 2519, Atomic Energy of Canada Ltd., Chalk River Nuclear Laboratories AECL, 1965.
[26] M. Harada, R. Wakamatsu, The effect of hydrogen on the transition behavior of the corrosion rate of zirconium alloys, Zirconium in the Nuclear Industry: 15th International Symposium, 2008, p. 384.
[27] E. Hillner, Hydrogen absoprtion in Zircaloy during aqueous corrosion, effect of environment, AEC Research and Development WAPD-TM-411, 1964.
[28] S. Kass, The development of the Zircaloys, Symposium on Corrosion of Zirconium Alloys, ANS Winter Meeting, 1963, New York, 1964, pp. 3–27.
[29] W.E. Berry, D.A. Vaughan, E.L. White, Hydrogen pickup during aqueous corrosion of zirconium alloys, Corrosion 17 (1961) 109.
[30] K. Une, K. Sakamoto, M. Aomi, J. Matsunaga, Y. Etoh, I. Takagi, et al., Hydrogen absorption mechanism of zirconium alloys based on characterization of oxide layer, Zirconium in the Nuclear Industry: 16th International Symposium, ASTM STP-1529, 2011, pp. 401–432.
[31] B. Cox, A mechanism for the hydrogen uptake process in zirconium alloys, J. Nucl. Mater. 264 (1999) 283–294.
[32] A. Couet, A.T. Motta, A. Ambard, The coupled current charge compensation model for zirconium alloy fuel cladding oxidation: I.Parabolic oxidation of zirconium alloys, Corros. Sci. 100 (2015) 73–84.
[33] A. Couet, A.T. Motta, A. Ambard, Oxide electronic conductivity and hydrogen pickup fraction in Zr alloys, Annual Meeting on Transactions of the American Nuclear Society and Embedded Topical Meeting: Nuclear Fuels and Structural Materials for the Next Generation Nuclear Reactors, NSFM 2014, , Reno, NV, 2014.
[34] B. Cox, Y.M. Wong, A hydrogen uptake micro-mechanism for Zr alloys, J. Nucl. Mater. 270 (1999) 134–146.
[35] M.S. Veshchunov, A.V. Berdyshev, Modelling of hydrogen absorption by zirconium alloys during high temperature oxidation in steam, J. Nucl. Mater. 255 (2–3) (1998) 250–262.
[36] M. Tupin, F. Martin, C. Bisor, R. Verlet, P. Bossis, J. Chene, et al., Hydrogen diffusion process in the oxides formed on zirconium alloys during corrosion in pressurized water reactor conditions, Corros. Sci. 116 (2017) 1–13.
[37] X. Wang, M.-J. Zheng, I. Szlufarska, D. Morgan, Continuum model for hydrogen pickup in zirconium alloys of LWR fuel cladding, J. Appl. Phys. 121 (2017).
[38] B.F. Kammenzind, Hydrogen pickup and redistribution in alpha-annealed Zircaloy-4, Zirconium in the Nuclear Industry: Eleventh International Symposium, ASTM STP-1295, 1996, pp. 338–370.
[39] B.F. Kammenzind, B.M. Berquist, R. Bajaj, P.H. Kreyns, D.G. Franklin, The long-range migration of hydrogen through Zircaloy in response to tensile and compressive stress gradients, Zirconium in the Nuclear Industry: Twelfth International Symposium, ASTM STP-1354, 2000, pp. 196–233.
[40] O.F. Courty, A.T. Motta, J.D. Hales, Modeling and simulation of hydrogen behavior in Zircaloy-4 fuel cladding, J. Nucl. Mater. 452 (2014) 311–320.
[41] O.F. Courty, A.T. Motta, C.J. Piotrowski, J.D. Almer, Hydride precipitation kinetics in Zircaloy-4 studied using synchrotron X-ray diffraction, J. Nucl. Mater. 461 (Jun 2015) 180–185.
[42] D.S. Stafford, Multidimensional simulations of hydrides during fuel rod lifecycle, J. Nucl. Mater. 466 (2015) 362–372, 2015/11/01/.
[43] G.M. Hood, Point defect diffusion in alpha-Zr, J. Nucl. Mater. 159 (1988) 149–175.
[44] C.E. Ells, C.J. Simpson, in: A.S.M. Metals Park (Ed.), Hydrogen in Metals, 1974, pp. 345–360.
[45] M.P. Puls, The Effect of Hydrogen and Hydrides on the Integrity of Zirconium Alloy Components: Delayed Hydride Cracking, Springer Verlag, London, 2012.
[46] M. Kerr, M.R. Daymond, R.A. Holt, J.D. Almer, S. Stafford, Scripta Mater. 62 (2010) 341–344.
[47] J. Cui, G.K. Shek, Z. Wang, J. Pressure Vessel Technol. 131 (2009) 041406.
[48] A. Sawatzky, The diffusion and solubililty of hydrogen in the alpha phase of Zircaloy 2, J. Nucl. Mater. 2 (1960) 62–68.
[49] J.J. Kearns, Diffusion coefficient of hydrogen in alpha zirconium, ziraloy-2 and zircaloy-4, J. Nucl. Mater. 43 (1972) 330–338.
[50] Y. Zhang, X.-M. Bai, J. Yu, M.R. Tonks, M.J. Noordhoek, S.R. Phillpot, Homogeneous hydride formation path in α-Zr: Molecular dynamics simulations with the charge-optimized many-body potential, Acta Mater. 111 (2016) 357–365, 2016/06/01/.
[51] S. Ishioka, M. Koiwa, Diffusion Coefficient in crystals with multiple jump frequencies, Philos. Mag. A 52 (1985) 267–277.
[52] Y. Zhang, C. Jiang, X.-M. Bai, Anisotropic hydriogen diffusion in alpha Zr and Zircaloy predicted by accelerated kinetic Monte Carlo simulations, Sci. Rep. 7 (2017) 1–13.
[53] C. Domain, Ab initio modelling of defect properties with substitutional and interstitials elements in steels and Zr alloys, J. Nucl. Mater. 351 (2006) 1–19.
[54] R.S. Daum, S. Majumdar, D.W. Bates, A.T. Motta, D.A. Koss, M.C. Billone, On the embrittlement of Zircaloy-4 under RIA-relevant conditions, Zirconium in the Nuclear Industry: Thirteenth International Symposium, ASTM STP-1423, 2002, pp. 702–718.
[55] A.M. Garde, G.P. Smith, R.C. Pirek, Effects of hydride precipitate localization and neutron fluence on the ductility of irradiated zircaloy-4, 11th International Symposium on Zr in the Nuclear Industry, ASTM STP 1295, Garmisch-Partenkirchen, 1996, pp. 407–430.
[56] A. Hellouin De Menibus, J. Sercombe, Q. Auzoux, C. Poussard, Thermo-mechanical loading applied on the cladding tube during the pellet cladding mechanical interaction phase of a rapid reactivity initiated accident, J. Nucl. Mater. 453 (2014) 210–213.
[57] M.C. Billone, T.A. Burtseva, R.E. Einziger, Ductile-to-brittle transition temperature for high-burnup cladding alloys exposed to simulated drying-storage conditions, J. Nucl. Mater. 433 (2013) 431–448, 2013/02/01/.
[58] A. McMinn, E.C. Darby, J.S. Schofield, The terminal solid solubility of hydrogen in zirconium alloys, 12th Int. Symp. on Zr in the Nuclear Industry, Toronto, CA, ASTM STP-1354, 2000, pp. 173–195.
[59] O. Zanellato, M. Preuss, J.Y. Buffiere, F. Ribeiro, A. Steuwer, J. Desquines, et al., Synchrotron diffraction study of dissolution and precipitation kinetics of hydrides in Zircaloy-4, J. Nucl. Mater. 420 (2012) 537–547, 1//.
[60] K. Une, S. Ishimoto, Dissolution and precipitation behavior of hydrides in Zircaloy-2 and high Fe Zircaloy, J. Nucl. Mater. 322 (2003) 66–72.
[61] K. Une, S. Ishimoto, Terminal solid solubility of hydrogen in unalloyed zirconium by differential scanning calorimetry, J. Nucl. Sci. Technol. 41 (2004) 949–952.
[62] P. Vizcaino, A.D. Banchik, J.P. Abriata, Solubility of hydrogen in Zircaloy-4: irradiation induced increase and thermal recovery, J. Nucl. Mater. 304

(2002) 96–106.
[63] W. Qin, N.A.P.K. Kumar, J.A. Szpunar, J. Kozinski, Intergranular δ-hydride nucleation and orientation in zirconium alloys, Acta Mater. 59 (2011) 7010–7021.
[64] E. Schelzke, Hydride orientation in Zircaloy tubes as a function of deformation texture and stresses, J. Nucl. Mater. 30 (1969) 324.
[65] R.S. Daum, Y.S. Chu, A.T. Motta, Identification and quantification of hydride phases in zircaloy-4 cladding using synchrotron radiation diffraction, J. Nucl. Mater. 392 (2009) 453–463.
[66] G. Östberg, Determination of hydride solubility in alpha phase zirconium, zircaloy-2 and zircaloy 4, J. Nucl. Mater. 5 (1962) 208–215, 1962/02/01/.
[67] E. Lacroix, A.T. Motta, J.D. Almer, Experimental determination of zirconium hydride precipitation and dissolution in zirconium alloy, J. Nucl. Mater. 509 (2018) 162–167, 2018/10/01/.
[68] M.P. Puls, The effects of misfit and external stresses on terminal solid solubility in hydride-forming metals, Acta Metall. 29 (1981) 1961–1968.
[69] G.F. Slattery, The mechanical properties of Zircaloy-2 tubing containing circumferentially aligned hydride, Applications-related Phenomena for Zirconium and its Alloys, ASTM STP-458, 1969, pp. 95–110.
[70] K.B. Colas, A.T. Motta, J.D. Almer, M.R. Daymond, M. Kerr, A.D. Banchik, et al., In situ study of hydride precipitation kinetics and re-orientation in Zircaloy using synchrotron radiation, Acta Mater. 58 (2010) 6575–6583.
[71] Z.L. Pan, I.G. Ritchie, M.P. Puls, Terminal solid solubility of hydrogen and deuterium in Zr-2.5Nb alloys, J. Nucl. Mater. 228 (1996) 227–237.
[72] K. Colas, A. Motta, M.R. Daymond, M. Kerr, J. Almer, Hydride platelet reorientation in zircaloy studied with synchrotron radiation diffraction, J. ASTM Int. (JAI) 8 (2011). Paper ID JAI103033.
[73] K. Colas, A. Motta, M. Daymond, J. Santisteban, P. Vizcaino, D. Banchik, et al., Kinetics of hydride precipitation in Zr alloys using synchrotron radiation, Presented at the CIAM Workshop in the VII Meeting of the Brazilian Society for Research in Materials (SBPMat), Guaruja, Brazil, 2008.
[74] M. Kerr, M.R. Daymond, R.A. Holt, J.D. Almer, Strain evolution of zirconium hydride embedded in a Zircaloy-2 matrix, J. Nucl. Mater. 380 (2008) 70–75.
[75] J.-I. Lin, X. Han, B.J. Heuser, J.D. Almer, Study of the mechanical behavior of the hydride blister/rim structure in Zircaloy-4 using in-situ synchrotron X-ray diffraction, J. Nucl. Mater. 471 (2016) 299–307, 2016/04/01/.
[76] M.N. Cinbiz, A.T. Motta, D. Koss, M. Billone, Hydride reorientation in zircaloy-4 under different states of stress as studied with in situ X-ray diffraction, Zirconium in the Nuclear Industry: 18th International Symposium, Astm International, West Conshohocken, ASTM STP-1597, 2018, pp. 1252–1285.
[77] C.E. Ells, Hydride precipitates in zirconium alloys (a review), J. Nucl. Mater. 28 (1968) 129–151.
[78] D.L. Douglass, The Metallurgy of Zirconium, International Atomic Energy Agency Supplement, Vienna, 1971.
[79] E. Zuzek, J.P. Abriata, A. San-Martin, F.D. Manchester, The H-Zr (hydrogen-zirconium) system, Bulletin of Alloy Phase Diagrams, vol. 11, 1990, pp. 385–395, 1990/08/01.
[80] Z. Zhao, M. Blat-Yrieix, J.P. Morniroli, A. Legris, L. Thuinet, Y. Kihn, et al., Characterization of zirconium hydrides and phase field approach to a mesoscopic-scale modeling of their precipitation, J. ASTM Int. (JAI) 5 (2008) p. JAI101161 (20 pp.), 03/01.
[81] H.M. Chung, R.S. Daum, J.M. Hiller, M.C. Billone, Characteristics of hydride precipitation and reorientation in spent-fuel cladding, Zirconium in the Nuclear Industry: Thirteenth International Symposium, ASTM STP-1423, 2002, pp. 561–582.
[82] R.P. Marshall, M.R. Louthan, Tensile properties of Zircaloy with oriented hydrides, Transactions of the ASM, vol. 56, 1963, pp. 693–700.
[83] J. Desquines, D. Drouan, M. Billone, M.P. Puls, P. March, S. Fourgeaud, et al., Influence of temperature and hydrogen content on stress-induced radial hydride precipitation in Zircaloy-4 cladding, J. Nucl. Mater. 453 (2014) 131–150, 2014/10/01/.
[84] M.N. Cinbiz, D.A. Koss, A.T. Motta, The influence of stress state on the reorientation of hydrides in a zirconium alloy, J. Nucl. Mater. 477 (2016) 157–164.
[85] R. Dutton, K. Nuttall, M.P. Puls, L.A. Simpson, Mechanisms of hydrogen induced delayed hydride cracking in hydride forming materials, Metallurgical Transactions A (Physical Metallurgy and Materials Science), vol. 8A, 1977, pp. 1553–1562.
[86] B.A. Cheadle, C.E. Coleman, J.F. Ambler, 7th International Symposium on Zr in the Nuclear Industry, Philadelphia, PA, ASTM STP-939, 1987, pp. 224–240.
[87] S. Sagat, S.Q. Shi, M.P. Puls, Crack initiation criterion at notches in Zr-2.5Nb alloys, Mater. Sci. Eng. 176 (1994) 237–247, 1994/3/31.
[88] K. Colas, A. Motta, M.R. Daymond, J. Almer, Mechanisms of hydride reorientation in zircaloy-4 studied in situ, Zirconium in the Nuclear Industry: 17th International Symposium, Hyderabad, India, ASTM STP-1543, 2014, pp. 1107–1137.
[89] G.J.C. Carpenter, J.F. Watters, In-situ study of the dissolution of gamma -zirconium hydride in zirconium, J. Nucl. Mater. 73 (1978) 190–197.
[90] G.J.C. Carpenter, The dilatational misfit of zirconium hydrides precipitated in zirconium, J. Nucl. Mater. 48 (1973) 264–266.
[91] K.B. Colas, A.T. Motta, M.R. Daymond, J.D. Almer, Effect of thermo-mechanical cycling on zirconium hydride reorientation studied in situ with synchrotron X-ray diffraction, J. Nucl. Mater. 440 (2013) 586–595.
[92] M.N. Cinbiz, D.A. Koss, A.T. Motta, J.-S. Park, J.D. Almer, In situ synchrotron X-ray diffraction study of hydrides in Zircaloy-4 during thermomechanical cycling, J. Nucl. Mater. 487 (2017) 247–259, 2017/04/15/.
[93] F. Garzarolli, W. Jung, H. Schoenfeld, A.M. Garde, G.W. Parry, P.G. Smerd, Waterside Corrosion of Zircaloy Fuel Rods, vol. 2789, Electric Power Research Institute EPRI-NP, 1982.
[94] G.P. Marino, Hydrogen supercharging in zircaloy, Mater. Sci. Eng. 7 (1971) 335–341.
[95] A. McMinn, E.C. Darby, J.S. Schofield, The terminal solid solubility of hydrogen in zirconium alloys, Zirconium in the Nuclear Industry: Twelfth International Symposium, vol. 1354, ASTM STP-1354, 2000, pp. 173–195.
[96] D. Gaston, C. Newman, G. Hansen, D. Lebrun-Grandié, MOOSE: a parallel computational framework for coupled systems of nonlinear equations, Nucl. Eng. Des. 239 (2009) 1768–1778.
[97] E. Lacroix, A.T. Motta, Validation of BISON calculation of hydrogen distribution by comparison to experiment, TMS2016 Annual Meeting Supplemental Proceedings, 2016, pp. 263–272.
[98] C. Domain, R. Besson, A. Legris, Atomic-scale ab-initio study of the Zr-H system: I. Bulk properties, Acta Mater. 50 (2002) 3513–3526.
[99] C. Domain, R. Besson, A. Legris, Atomic-scale ab initio study of the Zr-H system: II. Interaction of H with plane defects and mechanical properties, Acta Metall. 52 (2004) 1495–1502.
[100] P.A.T. Olsson, A.R. Massih, J. Blomqvist, A.M. Alvarez Holston, C. Bjerken, Ab initio thermodynamics of zirconium hydrides and deuterides, Comput. Mater. Sci. 86 (2014) 211–222.
[101] W. Zhu, R. Wang, G. Shu, P. Wu, H. Xiao, First-Principles study of different polymorphs of crystalline zirconium hydride, J. Phys. Chem. C 114 (2010) 22361–22368, 2010/12/23.
[102] X. Zhu, D.-Y. Lin, J. Fang, X.-Y. Gao, Y.-F. Zhao, H.-F. Song, Structure and thermodynamic properties of zirconium hydrides by structure search method and first principles calculations, Comput. Mater. Sci. 150 (2018) 77–85, 2018/07/01/.
[103] L. Thuinet, R. Besson, Ab initio study of competitive hydride formation in zirconium alloys, Intermetallics 20 (2012) 24–32, 2012/01/01/.
[104] M.A. Louchez, R. Besson, L. Thuinet, A. Legris, Interfacial properties of hydrides in α -Zr: a theoretical study, J. Phys. Condens. Matter 29 (2017) 415001.
[105] N. Moelans, B. Blanpain, P. Wollants, An introduction to phase-field modeling of microstructure evolution, Calphad 32 (2008) 268–294, 2008/06/01/.
[106] L.-Q. Chen, Phase-field models for microstructure evolution, Annu. Rev. Mater. Res. 32 (2002) 113–140, 2002/08/01.
[107] L. Thuinet, A. Legris, L. Zhang, A. Ambard, Mesoscale modeling of coherent zirconium hydride precipitation under an applied stress, J. Nucl. Mater. 438 (2013) 32–40, 2013/07/01/.
[108] L. Thuinet, A. De Backer, A. Legris, Phase-field modeling of precipitate evolution dynamics in elastically inhomogeneous low-symmetry systems: application to hydride precipitation in Zr, Acta Mater. 60 (2012) 5311–5321, 2012/08/01/.
[109] X.Q. Ma, S.Q. Shi, C.H. Woo, L.-Q. Chen, Simulation of gamma-hydride precipitation in bi-crystalline zirconium under uniformly applied load, Materials Science and Engineering A-Structural Materials Properties Microstructure and Processing, vol. 334, 2002, p. 6.
[110] X.H. Guo, S.Q. Shi, Q.M. Zhang, X.Q. Ma, An elastoplastic phase-field model for the evolution of hydride precipitation in zirconium. Part I: smooth specimen, J. Nucl. Mater. 378 (2008) 110.
[111] X.Q. Ma, S.Q. Shi, C.H. Woo, L.Q. Chen, The phase field model for hydrogen diffusion and γ-hydride precipitation in zirconium under non-uniformly applied stress, Mech. Mater. 38 (2006) 3–10, 2006/01/01/.
[112] X.H. Guo, S.Q. Shi, Q.M. Zhang, X.Q. Ma, An elastoplastic phase-field model for the evolution of hydride precipitation in zirconium. Part II: specimen with flaws, J. Nucl. Mater. 378 (2008) 120.
[113] X.Q. Ma, S.Q. Shi, C.H. Woo, L.-Q. Chen, Effect of applied load on nucleation and growth of gamma-hydrides in zirconium, Comput. Mater. Sci. 23 (2002) 283.
[114] S.-Q. Shi, Z. Xiao, A quantitative phase field model for hydride precipitation in zirconium alloys: Part I. Development of quantitative free energy functional, J. Nucl. Mater. 459 (2015) 323–329, 2015/04/01/.
[115] Z. Xiao, M. Hao, X. Guo, G. Tang, S.-Q. Shi, A quantitative phase field model for hydride precipitation in zirconium alloys: Part II. Modeling of temperature dependent hydride precipitation, J. Nucl. Mater. 459 (2015) 330–338, 2015/04/01/.
[116] J.E. Bailey, Electron microscope observations on the precipitation of zirconium hydride in zirconium, Acta Metall. 11 (1963) 267–280.
[117] A.M. Jokisaari, K. Thornton, General method for incorporating CALPHAD free energies of mixing into phase field models: application to the α-zirconium/δ-hydride system, Calphad 51 (2015) 334–343, 2015/12/01/.
[118] J. Bair, M. Asle Zaeem, D. Schwen, Formation path of δ hydrides in zirconium by multiphase field modeling, Acta Mater. 123 (2017) 235–244, 2017/01/15/.
[119] C. Shen, J.P. Simmons, Y. Wang, Effect of elastic interaction on nucleation: II. Implementation of strain energy of nucleus formation in the phase field method, Acta Mater. 55 (2007) 1457–1466, 2007/02/01/.
[120] C. Shen, J.P. Simmons, Y. Wang, Effect of elastic interaction on nucleation: I. Calculation of the strain energy of nucleus formation in an elastically anisotropic crystal of arbitrary microstructure, Acta Mater. 54 (2006) 5617–5630, 2006/12/01/.

[121] J.P. Simmons, C. Shen, Y. Wang, Phase field modeling of simultaneous nucleation and growth by explicitly incorporating nucleation events, Scripta Mater. 43 (2000) 935–942, 2000/10/30/.
[122] J.P. Simmons, Y. Wen, C. Shen, Y.Z. Wang, Microstructural development involving nucleation and growth phenomena simulated with the Phase Field method, Mater. Sci. Eng., A 365 (2004) 136–143, 2004/01/25/.
[123] A.M. Jokisaari, C. Permann, K. Thornton, A nucleation algorithm for the coupled conserved–nonconserved phase field model, Comput. Mater. Sci. 112 (2016) 128–138, 2016/02/01/.
[124] T.W. Heo, L.-Q. Chen, Phase-field modeling of nucleation in solid-state phase transformations, JOM 66 (2014) 1520–1528, 2014/08/01.
[125] T.W. Heo, L. Zhang, Q. Du, L.-Q. Chen, Incorporating diffuse-interface nuclei in phase-field simulations, Scripta Mater. 63 (2010) 8–11, 2010/07/01/.
[126] J. Bair, M. Asle Zaeem, M. Tonks, A review on hydride precipitation in zirconium alloys, J. Nucl. Mater. 466 (2015) 12–20, 2015/11/01/.
[127] B. Radhakrishnan, S.B. Gorti, K. Clamo, Y. Yan, Phase field simulations of hydride reorientation in Zircaloys, 14th International High-Level Radioactive Waste Management Conference: Integrating Storage, Transportation, and Disposal, IHLRWMC 2013, April 28, 2013 - May 2, 2013, Albuquerque, NM, United states, 2013, pp. 644–650.
[128] J.B. Bai, N. Ji, D. Gilbon, C. Prioul, D. Francois, Hydride embrittlement in Zircaloy-4 plate. Part II: interaction between the tensile stress and hydride morphology, Metall. Mater. Trans. 25A (1994) 1199–1208.
[129] J.B. Bai, C. Prioul, D. Francois, Hydride embrittlement in zircaloy-4 plate: Part I. Influence of microstructure on the hydride embrittlement in zircaloy-4 at 20 C and 350 C, Metall. Mater. Trans. 25A (1994) 1185–1197.
[130] S. Arsene, J. Bai, P. Bompard, Hydride embrittlement and irradiation effects on the hoop mechanical properties of pressurized water reactor (PWR) and boiling-water reactor (BWR) ZIRCALOY cladding tubes: Part III. Mechanical behavior of hydride in stress-relieved annealed and recrystallized ZIRCALOYs at 20C and 300C, Metall. Mater. Trans.: Phys. Metall. Mater. Sci. 34 A (2003) 579–588.
[131] M. Le Saux, J. Besson, S. Carassou, C. Poussard, X. Averty, Behavior and failure of uniformly hydrided Zircaloy-4 fuel claddings between 25 °C and 480 °C under various stress states, including RIA loading conditions, Eng. Fail. Anal. 17 (2010) 683–700.
[132] M. Le Saux, J. Besson, S. Carassou, A model to describe the mechanical behavior and the ductile failure of hydrided Zircaloy-4 fuel claddings between 25C and 480C, J. Nucl. Mater. 466 (2015) 43–55.
[133] M. Le Saux, J. Besson, S. Carassou, C. Poussard, X. Averty, A model to describe the anisotropic viscoplastic mechanical behavior of fresh and irradiated Zircaloy-4 fuel claddings under RIA loading conditions, J. Nucl. Mater. 378 (2008) 60–69.
[134] R.S. Daum, S. Majumdar, H.C. Tsai, M.C. Billone, D.W. Bates, D.A. Koss, et al., Embrittlement of hydrided zircaloy-4 under RIA-like conditions, 13th ASTM International Symposium on Zr in the Nuclear Industry, Annecy, France, ASTM STP-1423, 2001, pp. 702–719.
[135] V. Macdonald, S. Le Boulch, A. Hellouin de Menibus, J. Besson, Q. Auzoux, J. Crepin, et al., Procedia Mater. Sci. 3 (2014) 233–238.
[136] P.A. Raynaud, D.A. Koss, A.T. Motta, Crack growth in the through-thickness direction of hydrided thin-wall Zircaloy sheet, J. Nucl. Mater. 420 (2011) 69–82.
[137] T.M. Link, D.A. Koss, A.T. Motta, Failure of Zircaloy Cladding under transverse plane-strain deformation, Nucl. Eng. Des. 186 (1998) 379–394.
[138] Z. Marciniak, K. Kuczynski, Limit Strains in process of sheet forming metal, Int. J. Mech. Sci. 9 (1967) 609–620.
[139] Y. Rashid, R. Montgomery, Topical Report on Reactivity Initiated Accident: Bases for RIA Fuel Rod Failure and Core Coolability Criteria, EPRI, 2002, p. 1002865.
[140] J. Rashid, M. Rashid, A. Machiels, R. Dunham, A new material constitutive model for predicting cladding failure, Proceedings of Top Fuel Conference, 2009.
[141] Y. Rashid, M. Rashid, R. Dunham, Development of a Metal/hydride Mixture Model for Zircaloy Cladding with Mixed Hydride Structure, ANATECH Corp., Palo Alto, CA, 2004, p. 1009694.
[142] F. Perales, Y. Monerie, F. Dubois, L. Stainier, Computational non-smooth fracture dynamics in nonlinear and heterogeneous materials. Application to fracture of hydrided Zircaloy, 18th International Conference on Structural Mechanics in Reactor Technology (SMiRT 18), Beijing, China, August 7-12, 2005, 2005.
[143] S.Q. Shi, M.P. Puls, Fracture strength of hydride precipitates in Zr-2.5Nb alloys, J. Nucl. Mater. 275 (1999) 312–317.
[144] J.-S. Kim, T.-H. Kim, D.-H. Kook, Y.-S. Kim, Effects of hydride morphology on the embrittlement of Zircaloy-4 cladding, J. Nucl. Mater. 456 (2015) 235–245, 2015/01/01/.
[145] L.A. Simpson, C.K. Chow, Effect of metallurgical variables and temperature on the fracture toughness of zirconium alloy pressure tubes, Zirconium in the Nuclear Industry, ASTM STP-939, 1987, pp. 579–586.
[146] R.K. Sharma, S. Sunil, B.K. Kumawat, R.N. Singh, A. Tewari, B.P. Kashyap, Influence of hydride orientation on fracture toughness of CWSR Zr-2.5%Nb pressure tube material between RT and 300C, J. Nucl. Mater. 488 (2017) 231–244.
[147] M.N. Cinbiz, The Effect of Stress State on Zirconium Hydride Reorientation, Ph.D. Thesis in Nuclear Engineering, Penn State University, 2015.
[148] P. Raynaud, Crack Growth Through the Thickness of Thin-sheet Hydrided Zircaloy-4, Ph.D., Materials Science, Penn State University, 2009.
[149] S. Ziaei, Q. Wu, M.A. Zikry, Orientation relationships between coherent interfaces in hcp–fcc systems subjected to high strain-rate deformation and fracture modes, J. Mater. Res. 30 (2015) 2348–2359.
[150] H. Tummala, L. Capolungo, C.N. Tomé, Quantifying the stress state in the vicinity of a δ-hydride in α-zirconium, J. Nucl. Mater. 511 (2018) 406–416, 2018/12/01/.
[151] N. Capps, R. Montgomery, D. Sunderland, M. Pytel, B.D. Wirth, Evaluation of missing pellet surface geometry on cladding stress distribution and magnitude, Nucl. Eng. Des. 305 (2016) 51–63, 2016/08/15/.

Arthur Motta is Professor of Nuclear Engineering and Materials Science and Engineering and Chair of the Nuclear Engineering Program at Penn State University. He has worked in the area of zirconium alloy behavior, including radiation damage, corrosion, hydriding and mechanical properties for over 20 years.

Laurent Capolungo is a scientist at Los Alamos National Laboratory working on multi-scale modeling and characterization of metals in harsh environments. Using techniques such as discrete dislocation dynamics and cluster dynamics methods, Dr. Capolungo is particularly interested in studying plasticity and microstructure changes at the micron-scale and in using these studies to derive constitutive laws.

Long-Qing Chen is Donald W. Hamer Professor of Materials Science and Engineering, Professor of Engineering Science and Mechanics, and Professor of Mathematics at Penn State. He received his Ph.D. from MIT in Materials Science and Engineering in 1990 and joined the faculty at Penn State in 1992. He works in the area of computational microstructure evolution and multiscale modeling of structural metallic alloys, functional oxide thin films, and energy materials. He is the Editor-in-Chief for Computational Materials.

M. Nedim Cinbiz has a PhD degree in Nuclear Engineering from the Pennsylvania State University in 2015. His research focuses on zirconium hydride reorientation phenomena and effect of radial hydrides on the mechanical behavior of the zirconium alloys. He is currently a postdoctoral researcher at Oak Ridge National Laboratory performing research on the transient mechanical testing of advanced cladding candidates for light-water reactors.

The PI at Queen's University, **Mark Daymond,** is Canada Research Chair in Mechanics of Materials and Associate Industrial Research in Nuclear Materials with a specific focus on the mechanical properties of materials relevant to the life management of zirconium based alloys.

Donald Koss is Emeritus Professor of Materials Science at Penn State University. He has been involved in research addressing the mechanical behavior of a wide range of materials. Having published more than 175 papers, he has collaborated with Professor Motta in recent years on several programs addressing the deformation and fracture of zirconium-based alloys, particularly as influenced by hydrides.

Evrard Lacroix has a MSc in Nuclear Engineering from Penn State University and from Grenoble-INP Phelma and is a Ph.D. Student at Penn State University. His research focuses on understanding zirconium hydride precipitation and dissolution in zirconium alloys with the goal of modeling hydrogen behavior in nuclear fuel cladding.

Giovanni Pastore, Ph.D., is a research and development scientist at Idaho National Laboratory, where he leads the developers team for the nuclear fuel analysis code BISON. Dr. Pastore earned his master's degree in Nuclear Engineering (2008) and Ph.D. (2012) from the Politecnico di Milano (Italy). His research focuses on software development for engineering nuclear fuel performance analysis and on advanced modeling of fission gas behavior.

Pierre-Clement A Simon is a Ph.D. candidate at Penn State University in Nuclear Engineering with a background in Engineering Science and Applied Mathematics from Ecole Centrale de Lyon and Université Claude Bernard in France. His research focuses on the modeling of zirconium hydride morphology and orientation in nuclear fuel cladding using phase field modeling.

Dr. Michael R Tonks has a Ph. D. in Mechanical Engineering from the University of Illinois at Urbana-Champaign and is an Associate Professor of Materials Science and Engineering and Nuclear Engineering at the University of Florida. Prior to becoming a faculty member, he worked for seven years at Idaho National Laboratory. He has authored over 60 peer-reviewed publications in the areas of nuclear materials and computational materials science.

Brian Wirth is Governor's Chair Professor of Computational Nuclear Engineering at the University of Tennessee, Knoxville. His research investigates the performance of nuclear fuels and structural materials in nuclear environments. He has experience with various computational and experimental techniques to elucidate the dynamics of materials behavior from the nanometer to the continuum length scale.

Mohammed A. Zikry is the Zan Prevost Smith Professor at North Carolina State University in the Department of Mechanical and Aerospace Engineering. He is the editor in Chief of the ASME Journal of Engineering Materials and Technology. He received his Ph.D. from the University of California, San Diego, his M.S. from the Johns Hopkins University, and his B.S. from the University of Kansas.